JOURNAL OF GEOPHYSICAL RESEARCH, VOL. 104, NO. C1, PAGES 1431–1453, JANUARY 15, 1999

The connectivity of eddy variability in the Caribbean Sea, the Gulf of Mexico, and the Atlantic Ocean

Sylvia J. Murphy and Harley E. Hurlburt
Naval Research Laboratory, Stennis Space Center, Mississippi

James J. O'Brien
Center for Ocean Atmospheric Prediction Studies, Florida State University, Tallahassee

Abstract. A set of numerical simulations is used to investigate the connectivity of mesoscale variability in the Atlantic Ocean, the Caribbean, and the Gulf of Mexico. The primitive equation models used for these simulations have a free surface and realistic coastline geometry including a detailed representation of the Lesser Antilles island arc. Two simulations have 1/4° resolution and include a 5.5-layer reduced gravity and a 6-layer model with realistic bottom topography. Both are wind forced and include the global thermohaline circulation. The third simulation is from a 1/2° linear wind-driven model. In the two nonlinear numerical simulations, potential vorticity from decaying rings shed by the North Brazil Current retroflection can be advected through the Lesser Antilles. This potential vorticity acts as a finite amplitude perturbation for mixed barotropic and internal mode baroclinic instabilities, which amplify mesoscale features in the Caribbean. The eddies associated with the Caribbean Current are primarily anticyclonic and transit a narrow corridor across the Caribbean basin along an axis at 14° to 15°N with an average speed of 0.15 m/s. It takes them an average of 10 months to transit from the Lesser Antilles to the Yucatan Channel. Along the way, many of the eddies intensify greatly. The amount of intensification depends substantially on the strength of the Caribbean Current and is greatest during a multiyear period when the current is anomalously strong owing to interannual variation in the wind forcing. Some Caribbean eddies squeeze through the Yucatan Channel into the Gulf of Mexico, where they can influence the timing of Loop Current eddy-shedding events. There is a significant correlation of 0.45 between the Loop Current eddy shedding and the eddies near the Lesser Antilles with a time lag of 11 months. However, Caribbean eddies show no statistically significant net influence on the mean eddy-shedding period nor on the size and strength of shed eddies in the Gulf of Mexico. Additionally, no significant correlation is found between eddy shedding in the Gulf of Mexico and transport variations in the Florida Straits, although transport fluctuations in the Florida Straits at 27°N and the Yucatan Channel and showed a correlation of about 0.7 with a lag of 15 days. The linear solution exhibited a multiyear anomaly in the strength of the Caribbean circulation that was concentrated in the central and eastern Caribbean due to a multiyear anomaly in the wind field over the basin. In the nonlinear simulation this anomaly extended into the western Caribbean and across the entire Gulf of Mexico. This westward extension resulted from the nonlinearity and instability of the Caribbean Current, the westward propagation of the eddies, and the passage of Caribbean eddies through the Yucatan Channel into the Gulf of Mexico.

1. Introduction

The Caribbean is a semienclosed sea bounded on the east and the north by a chain of closely spaced islands that act as a sieve for inflow from the Atlantic Ocean. The islands from Guadaloupe south to Grenada (Figure 1) comprise the Lesser Antilles, while the larger islands to the north (Cuba, Hispaniola, and Puerto Rico) are referred to as the Greater Antilles. Westward flow between the islands of the Lesser Antilles enters the Caribbean and forms the westward flowing Caribbean Current (Figure 2), the principal current within the region. A great deal of uncertainty exists, however, about the distribution of inflow through the various Caribbean passages. The Caribbean Current exits the basin to the northwest through the Yucatan Channel and flows into the Gulf of Mexico to form the Loop Current (Figure 3). Both the Caribbean Current and the Loop Current are essential components of the Gulf Stream system, which is partly wind driven but which is also augmented by a contribution from the global thermohaline circulation [*Schmitz and Richardson*, 1991; *Schmitz*, 1995].

Many aspects of Caribbean circulation, including mesoscale variability, are summarized by *Kinder et al.* [1985]. *Maul* [1993] also presents an overview including the environmental and socioeconomic implications of global climate change in the Caribbean.

In this paper we investigate the connectivity of eddy variability in the Caribbean Sea, the Gulf of Mexico, and the

Paper number 1998JC900010.
0148-0227/99/1998JC900010$09.00

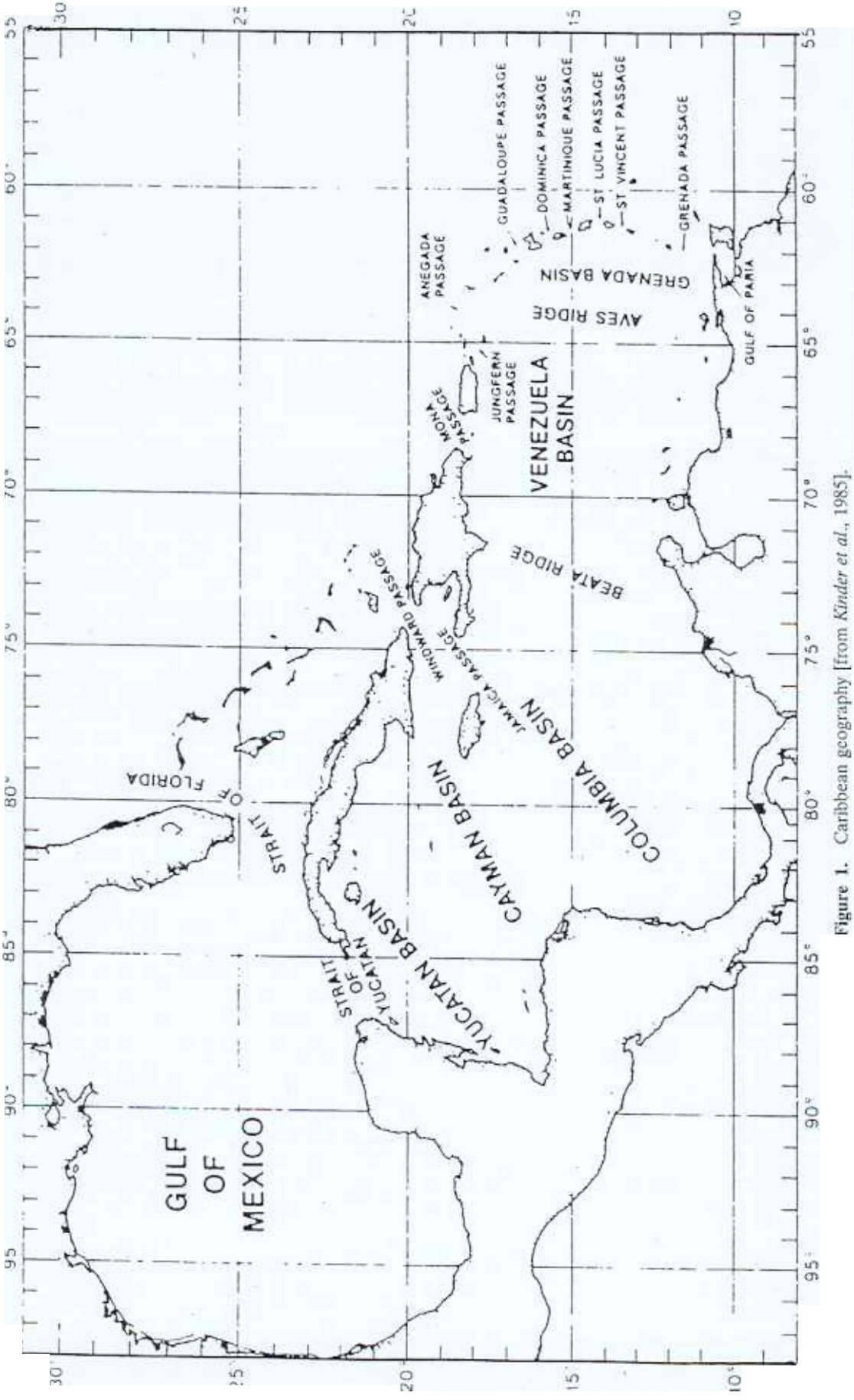

Figure 1. Caribbean geography [from *Kinder et al.*, 1985].

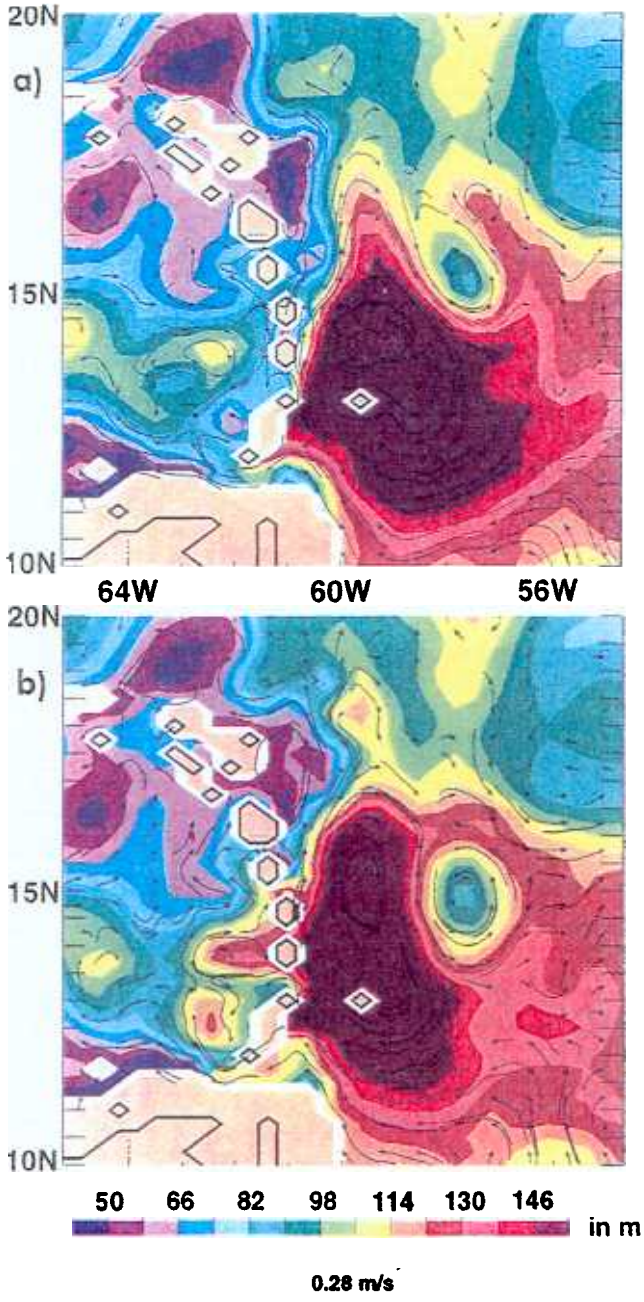

Plate 1. Snapshots of upper layer thickness (meters) and velocity vectors (meters per second) from simulation 1 for (a) September 2, 1992, where a ring from the North Brazil retroflection is impacting the Lesser Antilles, and (b) September 8, 1992, where potential vorticity from the ring is advected through the Lesser Antilles.

Atlantic Ocean. This includes (1) the influence of eddies that impinge on the eastern side of the Lesser Antilles, principally rings shed from the North Brazil Current retroflection [*Johns et al.*, 1990; *Fratantoni et al.*, 1995]; (2) the role of mesoscale flow instabilities in the Caribbean Current; and (3) the influence of the Caribbean eddies on eddy shedding by the Loop Current in the Gulf of Mexico, including eddies from the easternmost Caribbean.

Caribbean eddies have been discussed in the literature [*Fu and Holt*, 1983; *Heburn et al.*, 1982; *Ingham and Mahnken*, 1966; *Kinder*, 1983; *Lemming*, 1971; *Molinari et al.*, 1981; *Nystuen and Andrade*, 1993], but these studies have been limited in spatial and temporal resolution and coverage. The utilization of a global numerical model allows for research at time and space scales currently unfeasible observationally.

Three versions of the Naval Research Laboratory (NRL) Layered Ocean Model (NLOM) [*Wallcraft*, 1991] are used in this study. All are global in domain and contain detailed Caribbean geometry. The simulations include a reduced gravity, thermodynamic version (simulation 1, Table 1) with 1/4° resolution and a finite depth, hydrodynamic version (simulation 2, Table 1) also with 1/4° resolution. Finally, a linear, reduced gravity version (simulation 3, Table 1) with 1/2° resolution is utilized. After spin-up to statistical equilibrium, all of the simulations were forced by daily averaged winds from 1981 to 1994, so that interannual variability is also present. The formulation for the NLOM is presented in section 2 with detailed equations for the thermodynamic version. The modifications necessary to create a hydrodynamic version are also presented as well as a more detailed discussion of the design of the three simulations specifically used in this study.

These simulations contain different physics, which are used to include or exclude dynamical processes that may be relevant to the simulation of mean currents and variability in the Caribbean. For instance, simulation 2 contains realistic bottom topography. Simulation 1 is reduced gravity and therefore excludes the barotropic mode and the bottom topography. Since eddies are observed in both simulations, these differences provide a means to investigate (1) the influence bottom topography and baroclinic instability involving the barotropic mode on the simulated eddies in the Caribbean and (2) topographic effects on eddy formation and pathways of mean currents. Simulation 1 is also thermodynamic and therefore contains more accurate stratification that can influence eddy generation and propagation speeds. This simulation also has a more accurate representation of the return flow of the global thermohaline circulation, which affects the mean transports through the Lesser Antilles. The linear simulation excludes flow instability dynamics, providing a linear, deterministic ocean model response to the atmospheric forcing. It is used to demonstrate the impact of nonlinearity on a multiyear anomaly seen in the interannual simulations and to isolate the cause of this anomaly.

This investigation can be viewed as an attempt to use the model simulations to extend our understanding of a region with limited observations after comparing the simulations with the observational data currently available. However, additional observations are required to adequately assess the model results. Hence some of the results must be viewed as model predictions subject to future verification.

The connectivity of eddy variability in the Caribbean, Gulf of Mexico, and Atlantic Ocean is discussed in section 3. Topics include (1) the influence of the Atlantic Ocean on the formation of Caribbean eddies; (2) a description of the eddies, their mean pathways, and velocities; (3) a comparison between Caribbean eddies observed by Geosat altimetry and model eddies; (4) the relationship between Caribbean eddies and the eddy shedding from the Loop Current in the Gulf of Mexico; (5) discussion of an intradecadal cycle simulated in Caribbean variability and its potential origins; and, finally (6) a discussion of variability connectivity within the Gulf Stream system. Section 4 contains the summary and conclusions.

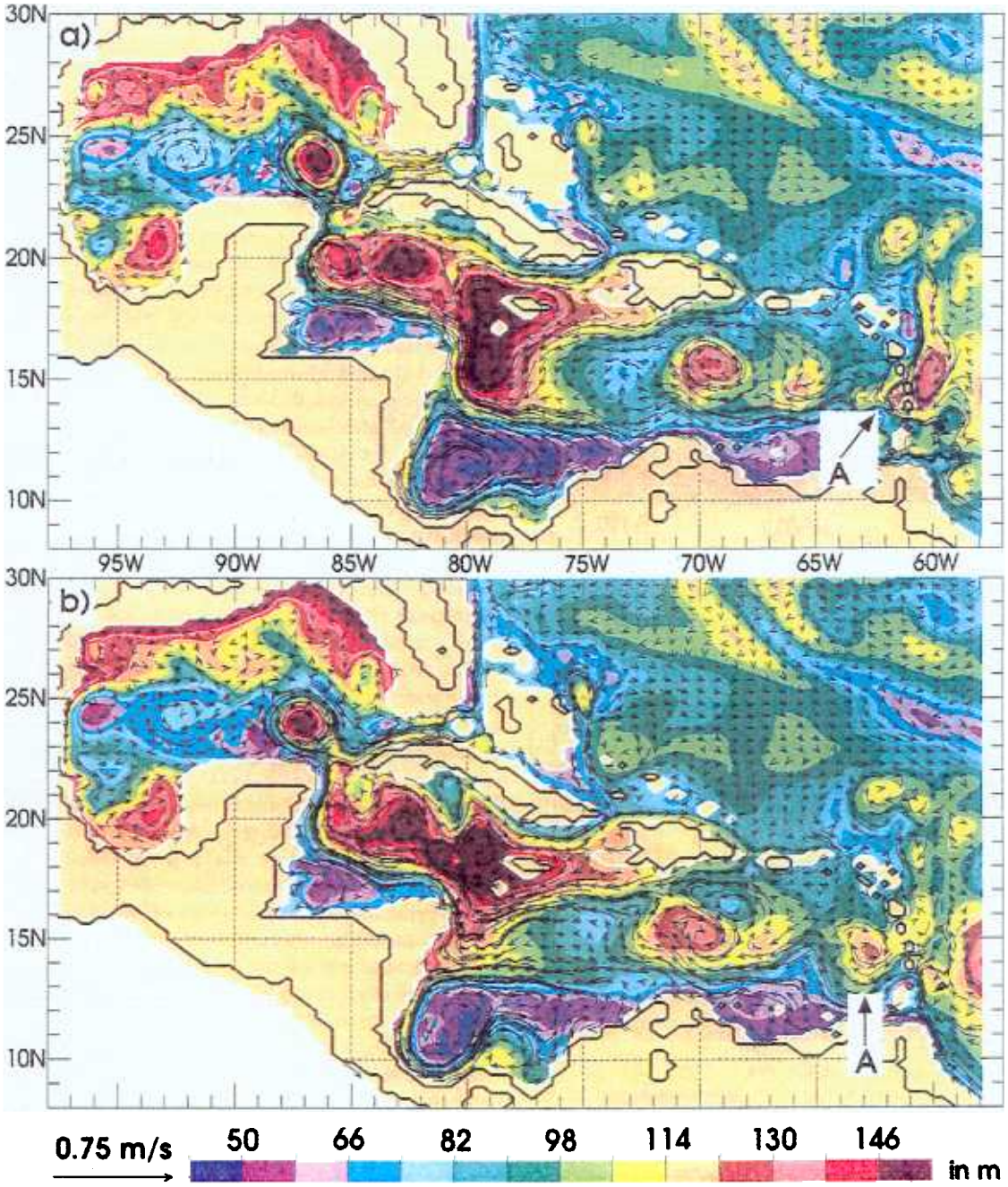

Plate 2. Snapshots of upper layer thickness (meters) and velocity vectors (meters per second) from simulation 1 on (a) August 18, 1991, when a North Brazil Current (NBC) ring impacts the Lesser Antilles, and (b) September 4, 1991, when fully formed eddy A is observed. The eddy labeled A is tracked through subsequent plots.

2. Ocean Model and Numerical Experiments

The NRL Layered Ocean Model [*Wallcraft*, 1991] is used for the numerical simulations in this study. It is based on the semi-implicit, free surface model of *Hurlburt and Thompson* [1980]. The model is formulated using an Arakawa C grid [*Mesinger and Arakawa*, 1976], an explicit numerical scheme for the reduced gravity simulations, and a semi-implicit scheme for the finite depth simulations. The equations for the n layer finite depth, thermodynamic model are, for layers $k = 1, \cdots, n$,

$$\frac{\partial \mathbf{V}_k}{\partial t} + (\nabla \cdot \mathbf{V}_k + \mathbf{V}_k \cdot \nabla)\mathbf{v}_k + \hat{k} \times f\mathbf{V}_k$$

$$= -h_k \sum_{l=1}^{n} [G_M \nabla(h_l - H_l) + h_l \nabla G_M]$$

$$- \frac{g}{\rho_0}\left(\sum_{l=1}^{k-1} h_l + \frac{h_k}{2}\right)\nabla\rho_k + (\tau_{k-1} - \tau_k)/\rho_0$$

$$+ \max(0, -\omega_{k-1})\mathbf{v}_{k-1} - [\max(0, \omega_{k-1})$$

$$+ \max(0, -\omega_k)]\mathbf{v}_k + \max(0, \omega_k)\mathbf{v}_{k+1}$$

$$+ \max(0, -C_M\omega_{k-1})(\mathbf{v}_{k-1} - \mathbf{v}_k)$$

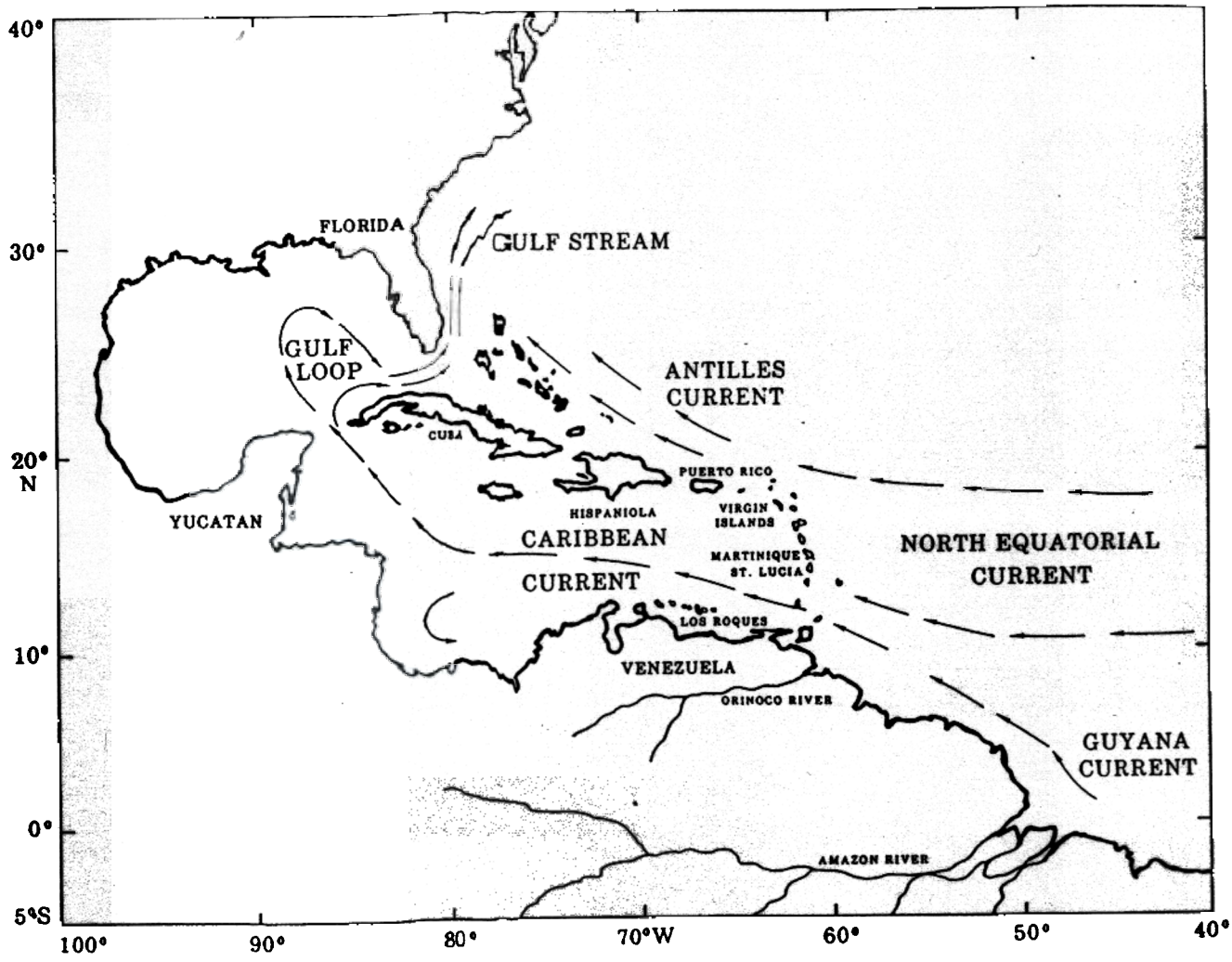

Figure 2. Schematic Caribbean circulation drawn from pilot charts [from *Duncan et al.*, 1982].

$$+ \max(0, C_M\omega_k)(\mathbf{v}_{k+1} - \mathbf{v}_k) + A_H\nabla^2\mathbf{V}_k$$

$$\frac{\partial h_k}{\partial t} + \nabla \cdot \mathbf{V}_k = \omega_k - \omega_{k-}$$

$$\frac{\partial \rho_k}{\partial t} + \mathbf{v}_k \cdot \nabla\rho_k = \frac{\max(0, \omega_k)}{h_k}(\rho_{k+1} - \rho_k)$$

$$+ \frac{\max(0, \omega_{k-1})}{h_k}(\rho_{k-1} - \rho_k) + \frac{H_0}{h_k}\sigma_\rho(\hat{\rho} - \rho_k)$$

$$- \delta_{lk}\frac{\gamma_l Q}{C_p\rho_0 h_l} + \frac{K_H}{h_k}\nabla \cdot (h_k\nabla\rho_k)$$

where

$$\nabla = \hat{\imath}\frac{1}{a\cos\theta}\frac{\partial}{\partial\phi} + \hat{\jmath}\frac{1}{a}\frac{\partial}{\partial\theta};$$

a radius of the Earth (6371 km);
A_H coefficient of horizontal eddy viscosity;
C_b coefficient of bottom friction;
C_f coefficient of interfacial friction;
C_M coefficient of additional interfacial friction associated with entrainment;
$D(\phi, \theta)$ ocean depth at rest;
f Coriolis parameter;
g acceleration due to gravity;
$G_{kl} = g$, $l \geq k$;
$G_{kl} = g - g(\rho_k - \rho_l)/\rho_0$, $l < k$;
h_k kth layer thickness;
h_k^+ kth layer thickness at which entrainment starts;
h_k^- kth layer thickness at which detrainment starts;
$H_0 = 100$ m and the reference layer thickness that forms part of a density relaxation e-folding timescale coefficient that equals $1/\sigma_\rho$ when $H_0 = h_k$;
H_k kth layer thickness at rest;
$H_n = D(\phi, \theta) - \Sigma_{l-1}^{n-1} H_l$;
$\hat{\imath}, \hat{\jmath}, \hat{k}$ unit vectors positive eastward, northward, and upward, respectively;
K_H coefficient of horizontal density diffusivity;
Q surface heat flux;
t time;
$\mathbf{v}_k$ kth layer velocity;
$\mathbf{V}_k$ $h_k\mathbf{v}_k$;
θ latitude;
ϕ longitude;
ρ_k kth layer density;
$\hat{\rho}(\phi, \theta)$ kth layer density climatology;

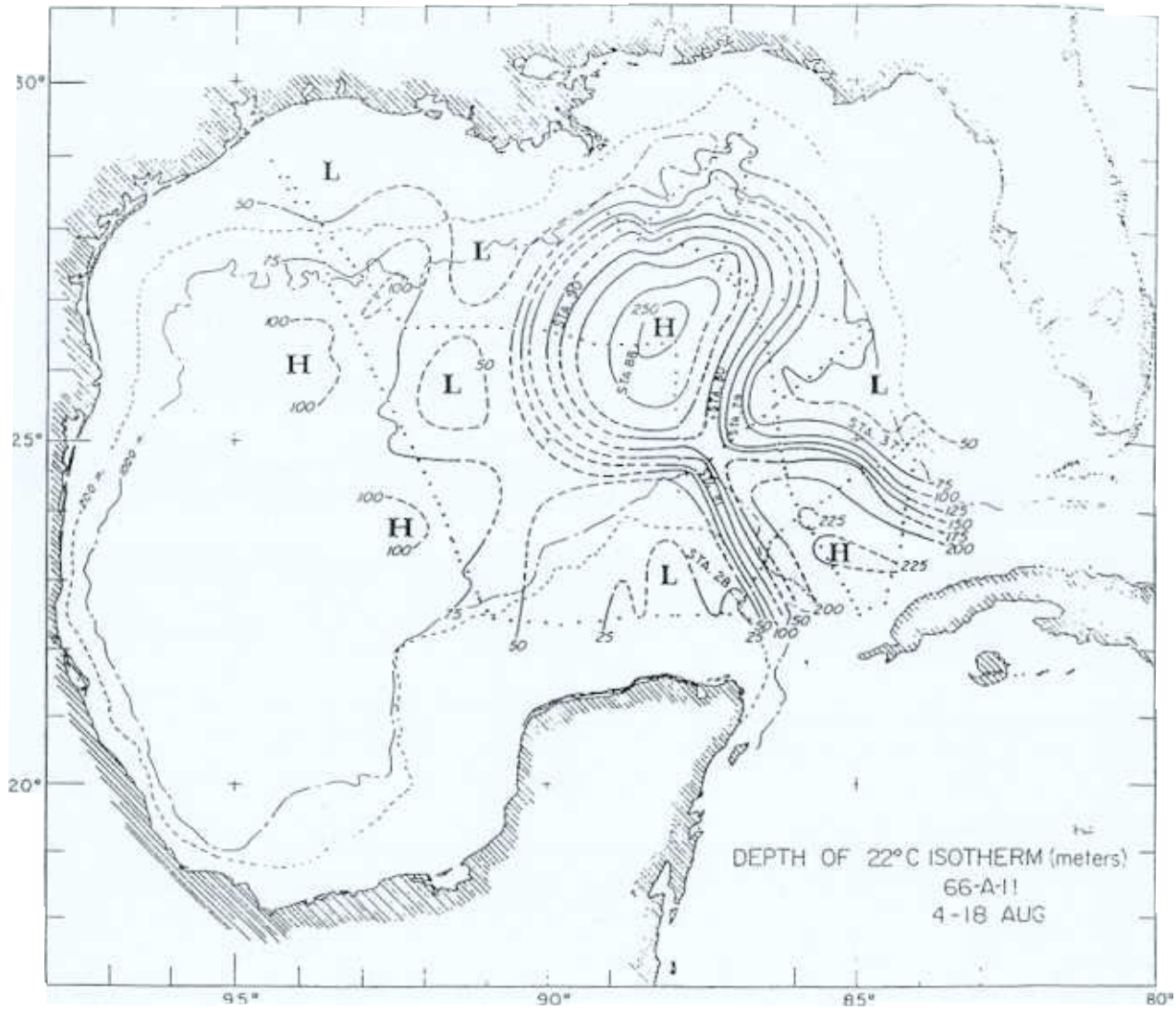

Figure 3. Topography of the 22°C isothermal surface, August 4–18, 1966 (Alaminos cruise 66-A-11) [from *Leipper*, 1970].

ρ_0 constant reference density;
σ_ρ reference coefficient of density climatology relaxation;
τ_w wind stress;
$\tau_k = \tau_w$, $k = 0$;
$\tau_k = C_k \rho_0 |v_k - v_{k+1}|(v_k - v_{k+1})$, $k = 1 \cdots n - 1$;
$\tau_k = C_b \rho_0 |v_n| v_n$, $k = n$;

$\omega_k = 0$, $k = 0, n$;
$\omega_k = \omega_k^+ - \omega_k^- - \Omega_k \hat{\omega}_k$, $k = 1 \cdots n - 1$;
$\omega_k^+ = \bar{\omega}_k [\max (0, h_k^+ - h_k)/h_k^+]^2$;
$\omega_k^- = \bar{\omega}_k [\max (0, h_k - h_k^-)/h_k^+]^2$;
$\hat{\omega}_k = \omega_k^+ \iint (\omega_k^+ - \omega_k^-)/\iint \Omega_k$;
$\bar{\omega}_k$ kth interface reference diapycnal mixing velocity;

Table 1 World Ocean Simulations

	Simulation		
		2	3
A, m²/s	300	300	500
Stratification σ, kg/m³	varies in time and space	25.24, 26.47, 26.99, 27.23, 27.39, 27.77	25.45, 27.55
Layers	5.5	6	1.5
Type	nonlinear, reduced gravity	nonlinear, realistic bottom	linear, reduced gravity
Thermohaline circulation,* Sv	14	8	not present
H_k	80, 160, 160, 250, 350, ∞	155, 185, 210, 225, 225, variable	250, ∞

A is coefficient of horizontal eddy viscosity; H_k is kth layer thickness at rest.
*North Atlantic outflow ports used have a net vertical profile of 1, 1, 2.1, 2.5, and 1.4 Sv (for $k = 1, \ldots, 5$)

Table 2. Additional Model Parameters

	Definition	Simulation 1	Simulation 2	Simulation 3
C_b	bottom drag coefficient	0	2×10^{-3}	0
C_k	kth interfacial stress coefficient	0	0	0
g, m/s^2	acceleration due to gravity	9.8	9.8	9.8
h_k^+, m	thickness of layer k at which entrainment starts	50 (k = 1), 40 (k = 2 5)	50 (k = 1), 40 (k = 2 , 5)	N/A
$\Delta\theta$, deg	latitudinal grid resolution	0.25	0.25	0.50
$\Delta\phi$, deg	longitudinal grid resolution	0.3515625	0.3515625	0.703125
ω_k, cm/s	kth interface vertical reference mixing velocity	0.001 for all layers	0.001 for all layers	N/A

N/A is not applicable.

$\Omega_k(\phi, \theta)$ kth interface weighting factor for global diapycnal mixing designed to conserve volume within a layer in compensation for explicit diapycnal mixing due to $h_k < h_k^+$ (e.g., $\omega_k^+ - \omega_k^-$) and net transport through the lateral boundaries of layer k.

A hydrodynamic version of this model is obtained by setting ρ = constant within a layer. This includes neglecting the density equation and retaining only the hydrodynamic part of the pressure gradient in the momentum equation:

$$\left[-h_k \sum_{l=1}^{n} G_{kl} \nabla (h_l - H_l) \right]$$

In reduced gravity simulations with n active layers, the equations are identical to the $(n + 1)$ layer finite depth equations, except that

H_n = constant
$G_{kl} = g(\rho_{n+1} - \rho_k)/\rho_0 \quad l \le k;$
$G_{kl} = g(\rho_{n+1} - \rho_l)/\rho_0 \quad l > k;$
$\tau_k = \tau_w, \; k = 0;$
$\tau_k = C_k \rho_0 |v_k - v_{k+1}|(v_k - v_{k+1}), \; k = 1 \cdots n;$
$\omega_k = 0 \quad k = 0;$
$\omega_k = \omega_k^+ - \omega_k^- - \Omega_k \hat{\omega}_k, \qquad k = 1 \cdots n.$

A modified version of the 1/2° ETOP05 bottom topography [*National Oceanic and Atmospheric Administration* (*NOAA*), 1986] was used in the finite depth simulation that included realistic bottom topography. The topography data set was first interpolated to the model grid and then smoothed with a nine-point real smoother. This smoothing is to reduce energy generation on small scales that are poorly resolved by the model.

The model includes realistic coastline geometry, based on ETOP05, which has been extensively modified in the Caribbean region by *Youtsey* [1993]. In most locations this geometry is determined by the 200-m depth contour of the topography, which is the minimum depth in the model and which represents the nominal shelf break. The model domain is global, excluding the Arctic, and extends from 72°S to 71°N. The horizontal resolution is 0.25° in latitude and 45/128° in longitude for each variable for the two main simulations and is 0.50° by 45/64° for the linear 1.5-layer reduced gravity simulation.

In the finite depth model simulation the amplitude of the topography above the maximum depth of 6500 m was multiplied by 0.78 to confine it to the lowest layer. This removes the numerical difficulty that arises when moving interfaces intersect sloping topography [*Hurlburt and Thompson*, 1980]. Flow through straits with a shallow sill is constrained to small values below the sill depth.

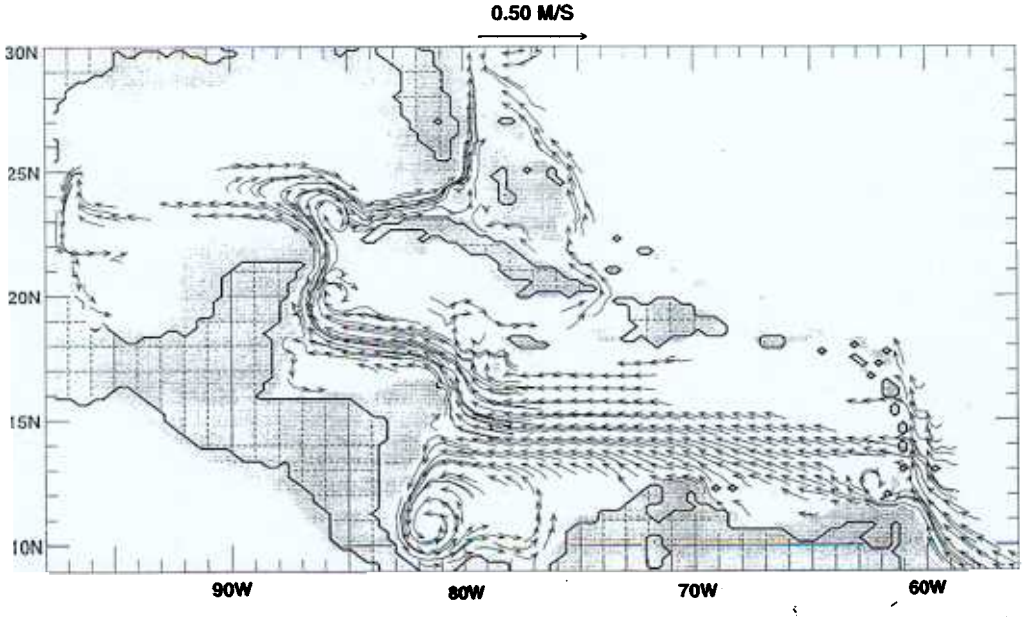

Figure 4. Mean currents over 1981–1991 for layer 1 of the nonlinear reduced gravity simulation.

Volume is conserved within each layer by requiring no net transfer of volume across each layer interface. The net volume flux across interface k, due to (1) outcropping and/or (2) any net transport of volume into or out of the layer above via ports in the lateral model boundaries, is balanced by the domain integral of cross-interfacial mixing across layer interface k ($\iint \Omega_k \hat{\omega}_k$). The weight function for this cross-interfacial mixing Ω_k is nonuniform in the NRL global model and has both positive and negative values based on oxygen saturation, as discussed in detail by *Shriver and Hurlburt* [1997]. This allows broad, slow upwelling over much of the world ocean interior in addition to regions of downwelling, e.g., the Labrador Sea. The model boundary conditions are kinematic and no slip at solid boundaries.

The thermal forcing in the thermodynamic version of the model is relaxation to annual mean density values derived from *Levitus* [1982]. Temporal variations in the layer interface depths are assumed to be nearly adiabatic. Therefore the density relaxation is always to the layer-averaged density based on layer interfaces at their temporal mean depth. Because most of the information about oceanic anomalies is contained in the interface depth, the density relaxation causes little damping of the oceanic anomalies and observationally verified anomalies in the thermodynamic simulation used here have been found that last for at least a decade [*Jacobs et al.*, 1994].

The model also includes interfacial friction that is quadratically proportional to the velocity shear between the adjacent layers. In the simulations used here, this type of interfacial friction is excluded by setting $C_k = 0$. However, an interfacial friction effect is retained via the diapycnal mixing.

Three versions of the model were used in this study. Table 1 provides details about their configurations, while other model parameters are listed in Table 2. The first simulation contains a representation of the first five baroclinic modes, while the second represents these modes plus the barotropic mode. The thermodynamic experiment was spun up from rest at 0.5° for 259 years and then at 0.25° for 36 years using the *Hellerman and Rosenstein* [1983] (hereinafter referred to as HR) monthly wind stress climatology. Similarly, the hydrodynamic experiment was spun up for 199 years at 0.5° and then for 29 years at 0.25°. The linear simulation was spun up until the annual mean reached a steady state, the two nonlinear simulations until they were near statistical equilibrium.

The simulations were then forced from 1981 to 1994 using winds from the European Centre for Medium-Range Weather Forecasts (ECMWF) [*ECMWF*, 1994] with the 1981–1994 ECMWF mean replaced by the Hellerman-Rosenstein annual mean. Use of this hybrid wind set is discussed by *Metzger et al.* [1992] and *Hurlburt et al.* [1996]. With the hybrid winds the long-term temporal mean is driven primarily by the HR winds, while the variability is driven by the ECMWF component and flow instabilities. The use of hybrid winds is compatible with the spin-up simulation, which was forced by the HR winds. The hybrid winds retain continuity in the temporal mean fields throughout the spin-up and the interannual portions of the simulations.

Both nonlinear simulations also include the global thermohaline circulation and the associated meridional overturning cell. This cell is driven primarily by deepwater formation in the far North Atlantic and by upwelling in the Antarctic Circumpolar Current (ACC) region [*Toggweiler and Samuels*, 1993; *Schmitz*, 1995; *Shriver and Hurlburt*, 1997]. These two regions of strong water mass transformation are connected by a southward Deep Western Boundary Current in the abyssal layer and by a northward return flow in the upper ocean which contributes 13 of the 32 Sv (1 Sv = 10^6 m^3 s^{-1}) through the Straits of Florida at 27°N [*Schmitz and Richardson*, 1991]. The relation of the Caribbean Sea to the region of the path of this return flow makes the global thermohaline circulation an essential element in this study.

In the model, deepwater formation is parameterized (1) by using ports along the northern boundary with prescribed outflow in the upper ocean and prescribed inflow in the abyssal layer and (2) by downwelling in the Labrador Sea via the oxygen-based cross-interfacial mixing scheme described earlier. Both simulations 1 and 2 have an imposed outflow of 8 Sv in the top five layers at two ports, one located between Greenland and Scotland, the second in the Davis Strait (Table 1). In the finite depth simulation (simulation 2), 8 Sv is injected into the bottom layer at ports located in the Denmark and Davis Straits. The remainder of the deepwater formation occurs via downwelling in the Labrador Sea with 6 Sv downward in simulation 1 and 1 Sv in simulation 2.

With respect to the return flow, the abyssal to upper ocean upwelling occurs primarily in the region of the ACC where all the model interfaces outcrop, although some occurs as broad, slow upwelling via the cross-interfacial mixing scheme. In the reduced gravity simulation the abyssal layer is infinitely deep and inert, but the upper ocean northward return flow branch of the global thermohaline circulation can still be included via the outflow port, downwelling in the subpolar Atlantic, the ACC upwelling, and the broad, slow cross-interfacial upwelling over the ocean interior. The resulting transport of the northward upper ocean return flow across 9°N is 14 Sv in simulation 1 (realistic based on the observational analysis of *Schmitz and Richardson* [1991]) and 9 Sv in simulation 2 (too weak). For a more comprehensive discussion of global thermohaline circulation simulation and dynamics in the NRL Layered Ocean Model, see *Shriver and Hurlburt* [1997].

The subdomains of the global model used for this study are (8.0°–31.0°N, 61.0°–100.0°W) for the reduced gravity simulation (simulation 1) and (0.0°–31.0°N, 45.0°–100°W) for the finite depth simulation (simulation 2) and the linear simulation (simulation 3). They comprise the Caribbean/Gulf of Mexico regions and part of the North Atlantic. Model output of both velocity components (u_k, v_k) and layer thickness anomaly ($h_k - H_k$) is available at every grid point at 3.05-day intervals for 14 years (1981–1994). In addition, time series of mass transport for each layer are output at daily intervals across selected sections, including the passages of the Caribbean. Comparison of simulated mean mass transport values with the available observational data from the region would provide a valuable assessment of the accuracy of the simulations. Unfortunately, transport data for passages of the Caribbean are limited, and few sets of existing surveys have produced highly variable results. *Mazeika et al.* [1983] indicated that this uncertainty was probably due to strong variations within the passages at tidal and subinertial scales, which means that any single shipboard occupation of a passage is unlikely to reproduce the mean. Additionally, some passages have been studied in greater detail than others, which results in an incomplete comparison.

Transports for the three southern most passages (Grenada, St. Vincent, and St. Lucia) have been reported as 9, 10, and 6 Sv, respectively (25 Sv total) [*Stalcup and Metcalf*, 1972; *Metcalf et al.*, 1971; *Stalcup et al.*, 1971], and 4.7, 3.4, and 0.9 Sv,

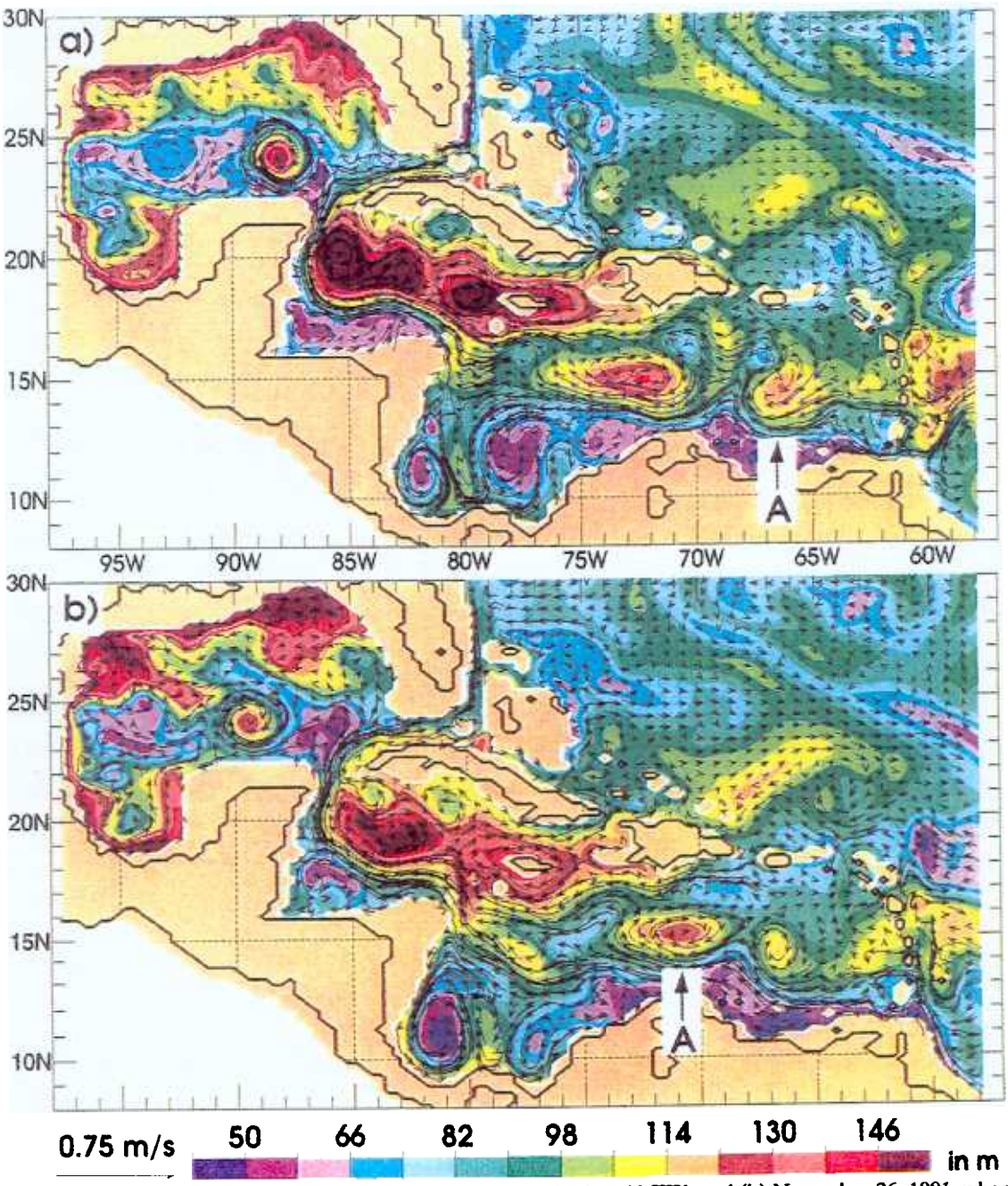

Plate 3. Eddy A on (a) October 6, 1991, when it has transited to 66.5°W, and (b) November 26, 1991, when it has transited to 71°W and intensified.

respectively (9.05 Sv total) [*Wilson and Johns*, 1997]. The corresponding simulated total mean transports from simulations 1 and 2 are 9.9 and 7.7 Sv, respectively.

Transport through Windward Passage has been estimated using an inverse model to have a mean inflow value of 7 Sv [*Roemmich*, 1981]. A more recent estimate is 4 Sv [*Schmitz*, 1996]. Both simulations have contradictory flows with mean outflow transports for simulations 1 and 2 of 0.8 and 3 Sv, respectively.

The mean transport of 29 Sv through Yucatan Channel has been estimated based upon its presumed contribution to the mean transport of the Florida Current [*Schmitz and Richardson*, 1991]. The mean simulated value of the Yucatan Channel transport for simulations 1 and 2 is 21.4 and 21.5 Sv, respectively.

The transport of the Florida Current has been quite accurately measured at 27°N [*Larsen*, 1992] with a mean value of 32.3 Sv. The model transport in this region for simulations 1 and 2 are 22.7 and 20.7 Sv, respectively.

The preceding comparisons indicate that in the southern Caribbean the simulations agree quite well with the latest observational data. Since this is where the Caribbean eddies form and intensify, this is an important conclusion. The discrepancies in the transports of the Florida Current at 27°N, the Yucatan Channel, and Windward Passage are caused by a known error in the topographic configuration of the eastern coastline of Florida and the geometry of the Bahamas [*Hurlburt and Townsend*, 1994] and do not affect the results presented in this paper regarding the transit of Caribbean eddies

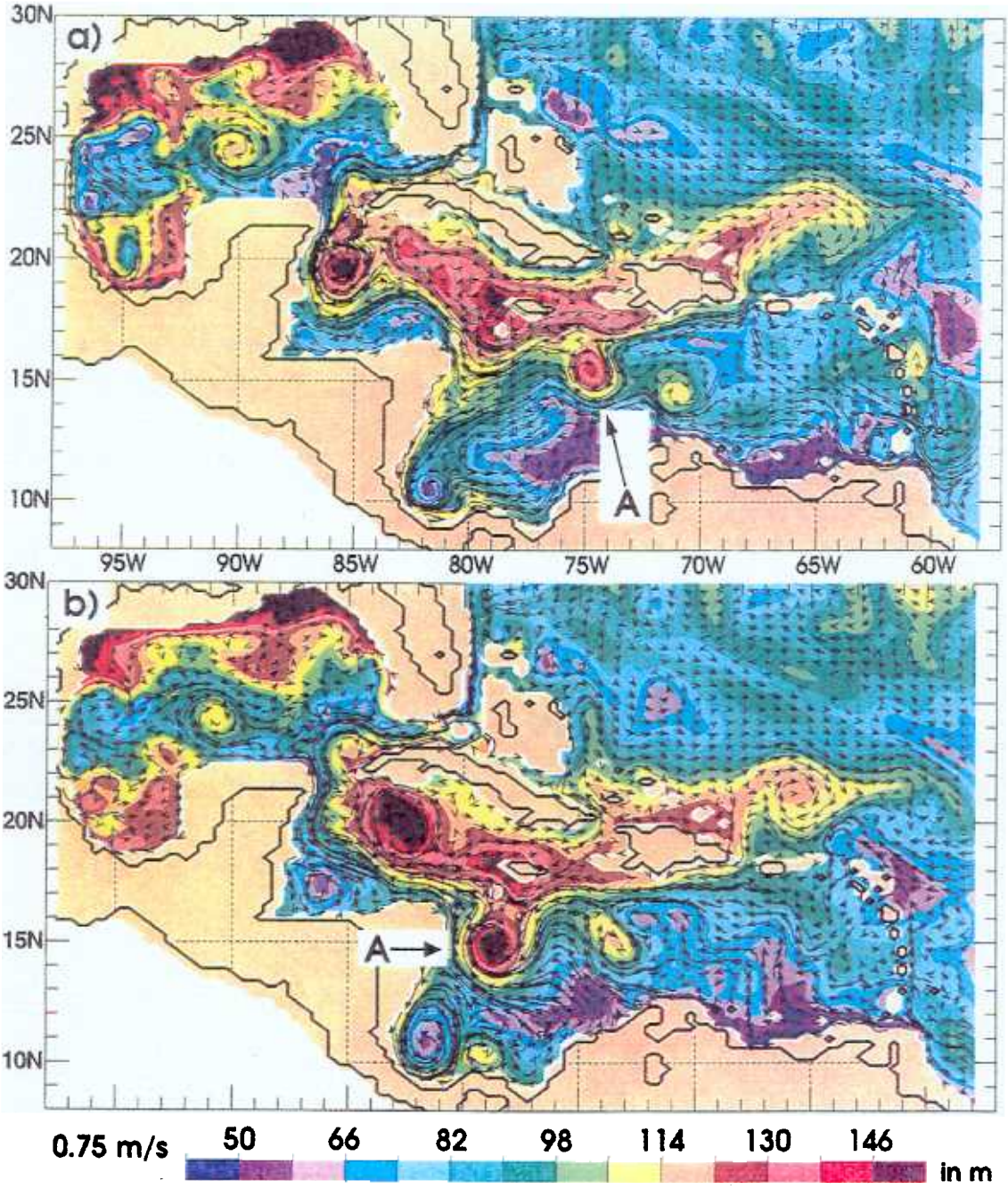

Plate 4. Eddy A on (a) January 4, 1992, when it is advected northwestward by the Caribbean Current to 75°W, and (b) February 16, 1992, when it is advected southwestward to 79°W.

into the Gulf of Mexico. This phenomenon has been simulated in other versions of the NRL model that possess accurate transports and topography in the western Caribbean, Bahamas, and Straits of Florida. Several of these versions are configured with significantly higher resolution than the ones used in this study, but unfortunately, none of these simulations was forced by daily interannual wind forcing for more than a decade.

All three of the model simulations described above are important to this study, although many of the results presented in the paper depend primarily upon simulation 1. Simulation 1 is more realistic because it is thermodynamic and has more accurate stratification than simulation 2. Simulation 1 also has a thinner upper layer; higher current velocities in this layer, which results in greater flow instabilities; higher eddy kinetic energy; and stronger Caribbean eddies. As will be discussed later, flow instabilities are required to demonstrate the North Brazil Current ring and Caribbean eddy connectivity that is the primary focus of this paper. Additionally, by using a reduced gravity simulation, we are able to show that bottom topography and baroclinic instability between the barotropic and the internal modes are not essential in our results and, in fact, play no role. Simulation 1 also has a more accurate representation of the return flow of the global thermohaline circulation, which also results in higher eddy kinetic energy as well as more accurate mass transport through the passages of the Lesser Antilles.

Simulation 3 has a very specific purpose in this paper. It is used (1) to isolate the cause of an anomaly in the Caribbean Current (discussed later) because any anomalies in this simu-

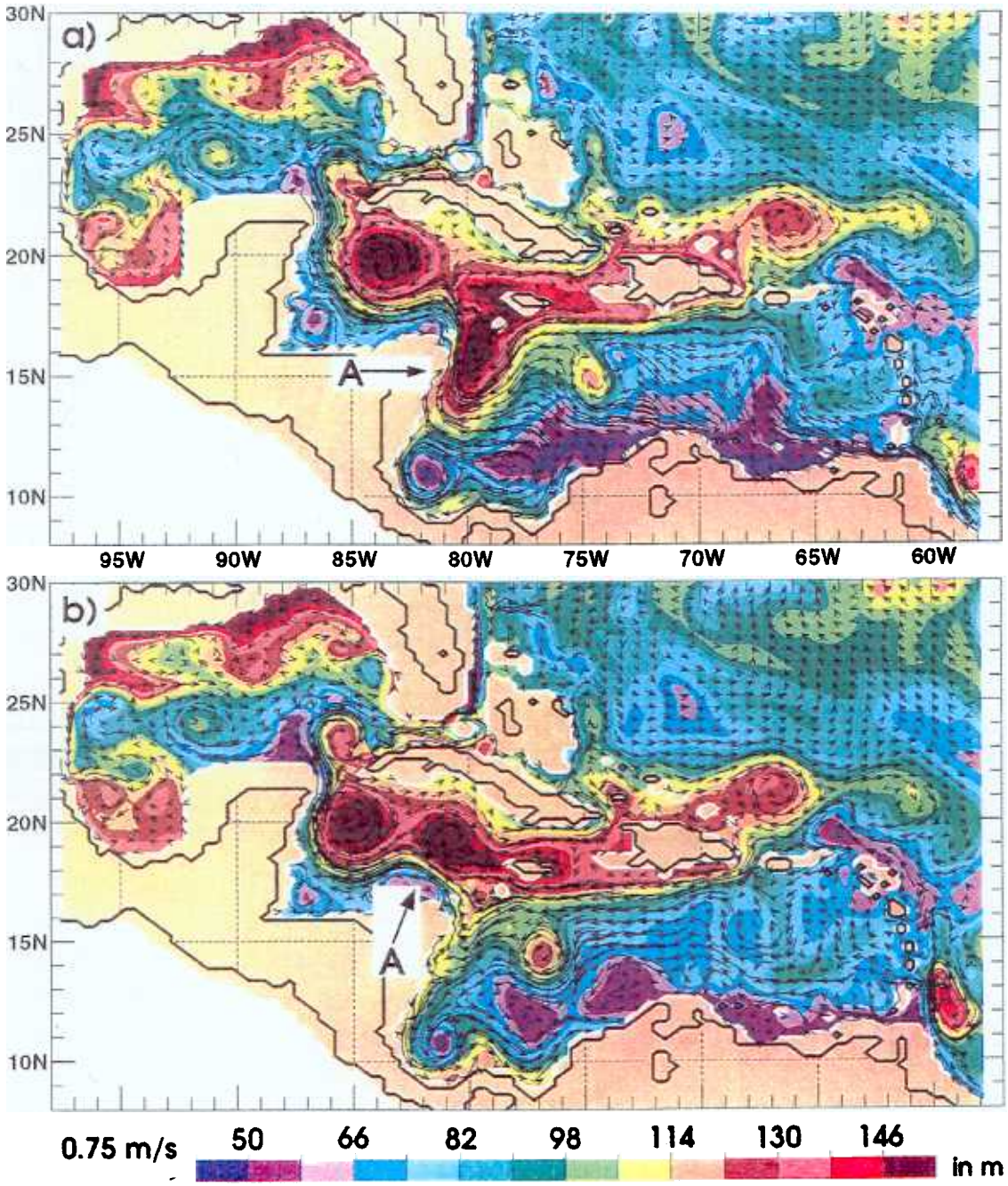

Plate 5. Eddy A on (a) March 3, 1992, when it moves northward and starts to merge with a large eddy west of Jamaica, and (b) March 28, 1992, when the merged eddy transits to 81°W.

lation are a linear, deterministic response to the atmospheric forcing, and (2) to help demonstrate the impact of nonlinearity and eddies on this anomaly.

3. Results

3.1. NBC Rings and Caribbean Eddy Formation

The mean Caribbean circulation represented in Figure 2 is simulated by the numerical model including the Caribbean Current, cyclonic circulation in the Colombian Basin, and the Loop Current in the Gulf of Mexico (Figure 4).

Mesoscale features in the Caribbean are observed in both nonlinear model simulations. The formation of these features is due in part to potential vorticity being advected through the Lesser Antilles from the Atlantic Ocean. The source of this potential vorticity can be seen in Plate 1a, where a large anticyclonic ring shed from the retroflection of the North Brazil Current (NBC) is observed in the model on the eastern side of the Lesser Antilles. Plate 1b demonstrates flow from the NBC ring into the Caribbean and the formation of an eddy on the western side of the Lesser Antilles. An analysis of potential vorticity for 1986 on either side of St. Vincent passage resulted in a cross-correlation value of 0.54 at lag 90 days for simulation 1. This indicates that potential vorticity is not a constant through the passage, and at least some of the vorticity from the eastern side is advected to the west.

Since a pioneering investigation into NBC rings by *Johns et al.* [1990], they have been observed in Geosat data [*Didden and*

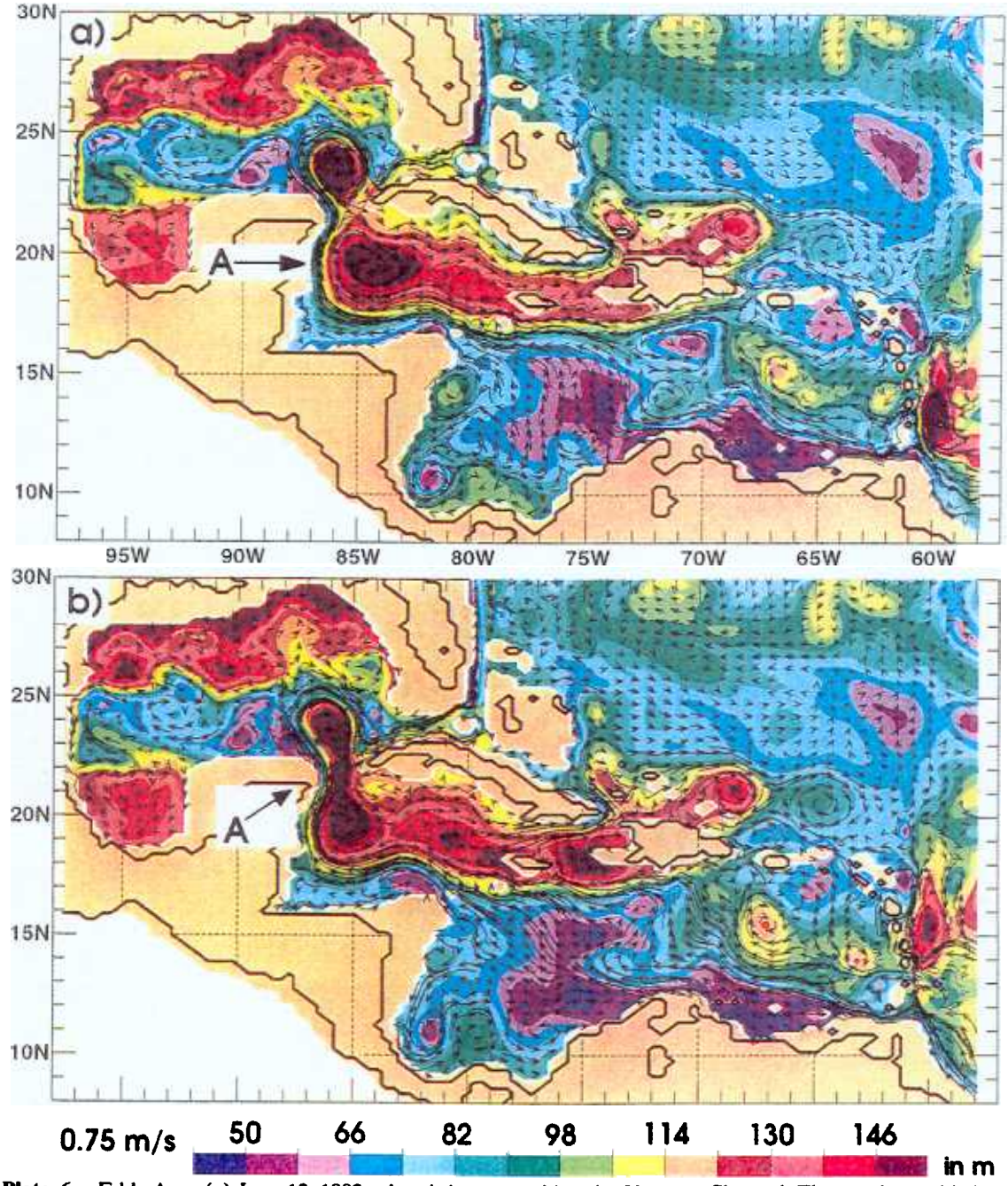

Plate 6. Eddy A on (a) June 12, 1992, when it is approaching the Yucatan Channel. The previous eddy has transited through the Yucatan Channel and into the Loop Current Eddy. (b) Eddy A on June 27, 1992, when material from the leading edge of it passes through the Yucatan Channel into the Loop Current.

Schott, 1993], by drifters [*Richardson et al.*, 1994], by current meter arrays, and in numerical models [*Fratantoni et al.*, 1995]. In all of these studies, approximately three NBC rings per year transit up the coast toward the Lesser Antilles. *Fratantoni et al.* [1995] reported that both the observed and modeled eddies decayed within 120 days of reaching the ridge between Tobago and Barbados (essentially the Lesser Antilles). It appears from the model simulation (Plate 1) that as the NBC rings decay, some of their vorticity can be advected into the Caribbean.

3.2. Eddy Amplification Within the Caribbean

The initial eddy formation is weak, but the potential vorticity advected through St. Vincent passage is a finite amplitude perturbation on which flow instabilities can grow. A beta Rossby number analysis of both nonlinear simulations was used as one test of the hypothesis that the eddies form as a result of barotropic instability. The beta Rossby number is defined as $v/\beta r^2$, where v is the maximum swirl velocity of an eddy averaged around the eddy, β is the variation of the Coriolis parameter with latitude, and r is the mean radius of the eddy from the center to the maximum swirl velocity. The diameter ($2r$) and maximum swirl velocities were determined for six representative eddies. The average diameter for simulation 1 was 330 km, and for simulation 2 it was 365 km. The beta Rossby numbers for these eddies were order 1 for both simulations with an average of 0.47 for simulation 1 and 0.77 for

simulation 2. A beta Rossby number of the order of 10 is indicative of baroclinic instability involving the barotropic mode, while a beta Rossby number of order 1 is indicative of an equivalent barotropic instability of the first baroclinic mode [see *McWilliams and Flierl*, 1979; *Hurlburt and Thompson*, 1982, 1984].

The low beta Rossby number in both simulations 1 and 2, the similarity of the eddies in the two simulations, and the similarity of the eddy trajectories serve as justification for studying the Caribbean eddies with a reduced gravity simulation. These similarities imply that there is little or no baroclinic instability between the barotropic and first baroclinic modes nor influence of the bottom topography. However, a vertical analysis of layer thickness anomaly revealed a mixture of barotropic and internal mode baroclinic instability between layers 1 and 2. This was indicated by some eddies being barotropic with depth while others were baroclinic while they strengthened. Additionally, several eddies were observed to change from barotropic to baroclinic and back again in the course of a life cycle. Finally, one double-lobed eddy was observed with one lobe baroclinic with depth and the other barotropic. Note that this analysis was performed during periods of eddy intensification.

3.3. Life Cycle of Caribbean Eddies

The resulting anticyclonic eddies are observed to transit from the Lesser Antilles along an axis of 14°–16°N until they are deflected northward by the Nicaraguan coast (Plates 2–5). Here the eddies often merge and intensify until they pass through the Yucatan channel (Plate 6b).

Plates 2–7 are a sequence of model snapshots that represent a case study for a typical anticyclonic eddy track through the Caribbean from simulation 1. Snapshots are available at the frequency of the model output (3.05 days), and the position of the eddy has been conclusively verified in every snapshot. For the sake of brevity, however, only 12 out of the possible 100 snapshots are presented.

Plate 2a shows an NBC ring impacting the Lesser Antilles with flow from the ring entering the Caribbean. The eddy that is beginning to form on the western side of the islands has been labeled eddy A. In Plate 2b a fully formed eddy A is observed. In Plates 3a and 3b, eddy A is observed to continue its westward transit and it begins to intensify. This intensification is due to flow instabilities of the Caribbean Current. In Plates 4a and 4b the path of eddy A is perturbed first northward and then southward by the Caribbean Current. Eddy A begins to merge with the large eddy near Jamaica (Plate 5a). In Plate 5b the merged eddy A has transited farther westward. Note also that in Plate 5b, there is a large eddy west of eddy A. In Plate 6a the eddy west of eddy A has squeezed through the Yucatan Channel. In this figure, eddy A transits to the Yucatan Channel. In Plate 6b the leading edge of eddy A is squeezing through the Yucatan Channel, but as we can see from Plate 7a, the entire eddy does not make the transit before the Loop Current Eddy is shed. In Plate 7b the Loop Current Eddy is making its westward transit across the Gulf of Mexico. This eddy is labeled eddy A since part but not all of eddy A is present. This particular eddy track was chosen, because it shows a wide variety of typical features associated with the simulated Caribbean eddies, including (1) formation from an NBC ring fragment that passes into the Caribbean through a narrow passage in the Lesser Antilles, (2) intensification due to instability of the Caribbean Current as it propagates westward through the Caribbean, (3) eddy merging, and (4) passage of part of the eddy through the Yucatan Channel. Also, it is easily followed on a Hopfmuller diagram of eddy tracks (section 3.5).

Many Caribbean eddies only exhibit some of the features seen during the life span of eddy A. Compared with other Caribbean eddies, however, eddy A is not one of the strongest, nor is it the most dramatic example of NBC ring intrusion into the Caribbean nor of an eddy passing through the Yucatan Channel and influencing eddy shedding in the Gulf of Mexico. Many of these points are discussed in greater detail throughout the remainder of section 3.

On average, an eddy takes approximately 10 months to transit the basin. Throughout Plates 2–7 other anticyclonic eddies can be seen in various stages of transit. This is indicative of the complex and continuous flow of mesoscale variability that crosses the region.

3.4. Model Data Comparison

There is a paucity of observational data in the Caribbean with which to conduct model-data comparisons. In one case, eddies observed in the reduced gravity simulation can be related to eddies observed by Geosat. It should be noted that the model eddies are not caused by a deterministic response to the atmospheric forcing, and therefore a comparison between observed and modeled eddies can be done only in a statistical sense, not as individual eddies. *Nystuen and Andrade* [1993] reported two eddy tracks (Figure 5) over a 1-month time span: June–July 1987 and April–May 1988. The Geosat eddy A (1987) tracks approximately 1° farther south and 2° farther west than the model eddy A (Figure 6a).

For the second Geosat sequence (Figure 6b), satellite eddy C tracks 1° farther north and 2° farther east than the model eddy C (Figure 6b). Intensity variations are approximately the same as the previous sequence.

3.5. Caribbean Eddy Trajectories

The model-simulated anticyclonic Caribbean eddies transit westward in a fairly narrow corridor. This corridor was determined by tracking upper layer thickness maxima averaged within a sequence of small rectangular boxes along the corridor. The size of each box was chosen to best capture the average pathway of the maxima so that the corridor encompassed most of the ensemble of eddy tracks. There are a total of 32 rectangles, each containing a time series of upper layer thickness averaged over the box (12 years long). The long-term mean (1981–1992) is subtracted. Figure 7 depicts these boxes, shaded together to illustrate the corridor.

A phase plot of the upper layer thickness anomalies along the corridor for simulation 1 (Plate 8) clearly traces the Caribbean eddies from the Lesser Antilles (0 km) through the Yucatan Channel (3000 km) and into the Loop Current eddy-shedding regime. The propagation speed of the eddies along the track is fairly uniform for the first 2000 km of the track. At 2000 km (approximately 80°W) the track turns northward and the eddies intensify and accelerate. The average propagation speed to the Yucatan Channel (3000 km) is 0.15 m/s. The average transit time from the Lesser Antilles to the Yucatan Channel is 10 months, with values as short as 7 months and as long as 17 months. The black dots starting in 1991 in Plate 8 correspond to the positions of eddy A observed in Plates 2–7, while the black square corresponds to the Loop Current Eddy observed in Plate 7b. Plate 8 also demonstrates that only part

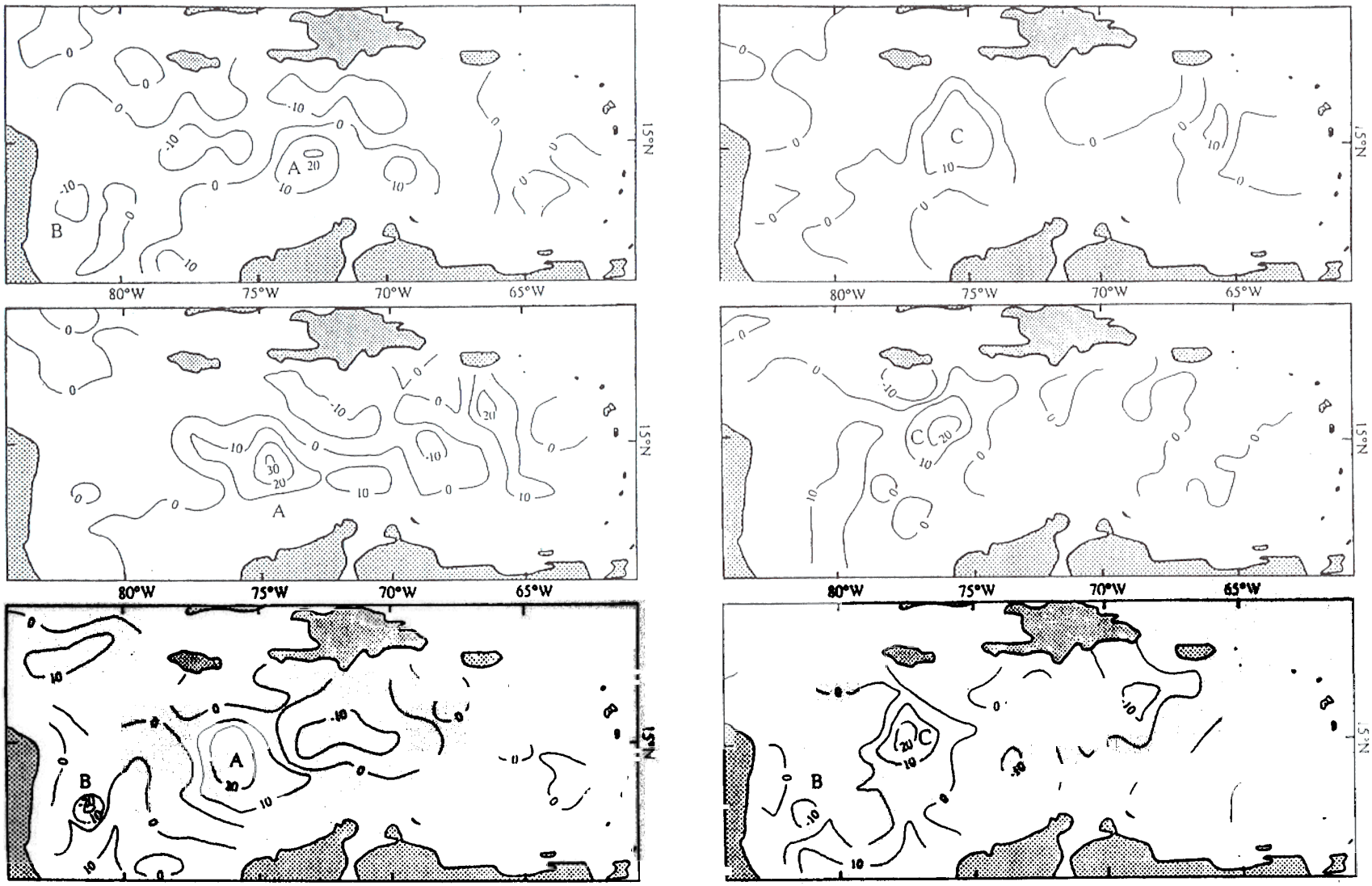

Figure 5. Geosat sea surface height (SSH) anomalies [from *Nystuen and Andrade*, 1993] on (left) June 17, July 4, and July 21, 1987, and (right) April 13, April 30, and May 17, 1988. Contour interval is 10 cm.

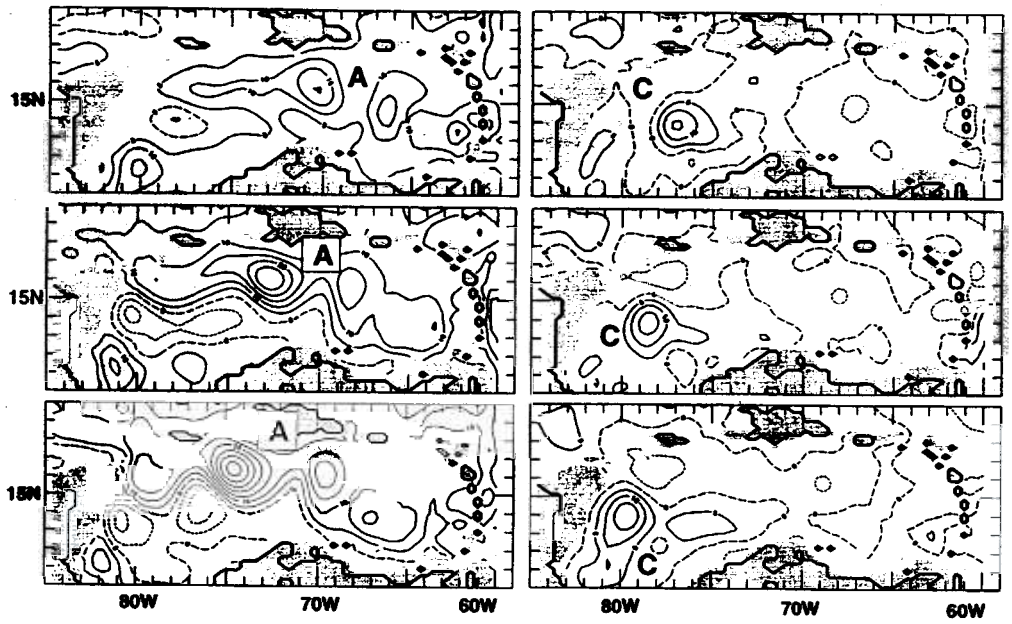

Figure 6. SSH anomalies, corresponding in time with Figure 5, from simulation 1. Contour interval is 10 cm, and dashed lines are negative contours.

of eddy A transits the Yucatan Channel. Part of the eddy west of eddy A also transits through the Yucatan channel (Plate 5b). That eddy transits the entire Caribbean but does not stay on the average eddy track which is depicted graphically in Figure 7; so there is a false break in the resulting track depicted in Plate 8. The corresponding plot for simulation 2 (Plate 9) is similar, except for the frequency of eddy shedding by the Loop Current.

Figure 7. Path representing the average eddy track through the Caribbean.

3.6. Loop Current Eddy Shedding

The observed frequency for separation of the Loop Current eddies is of the order of a year. The data sets of ring separations are gappy, the eddy-shedding period varies, and an insufficient number of ring separations have been observed. This hinders statistical analysis, and different analyses show different spectral peaks. For example, *Vukovich* [1995] compiled two data sets, one 22-year data set (1972–1993) and one 17-year data set (1977–1993), from various sources. *Sturges* [1992] also reported a technique to develop a continuous data set. Sturges found a primary spectral peak at 8.5 months and secondary peaks at 6, 13.4, and 25 months. Multiple spectral peaks were also reported by *Vukovich* [1988], *Maul and Vukovich* [1993] (6, 10.9, and 17 months), and *Vukovich* [1995] (9, 14 months). A single frequency of 8–9 months was reported by *Maul et al.* [1985].

It is unclear whether this variability in frequency reflects the natural variability of ring separation or problems associated with the data sets, such as their length. For example, *Vukovich* [1995] reported a primary spectral peak at 9 months and a secondary peak at 14 months. The mean period of the Loop Current eddy shedding (11 months) would have a frequency equal to the secondary spectral peak, with only one more data occurrence at 11 months, and it would have a frequency equal to the primary spectral peak with only two more data occurrences.

In the 12.5 years of reduced gravity model results, there were 18 Loop Current eddies. This number was determined by averaging the reduced gravity upper layer anomalies at 89.8°W from 21.0 to 30.0°N (Plate 10). This resulted in a mean period of 8.3 months between eddies. In the finite depth simulation there were 24 eddies in 12 years (Plate 9) or an average of 6.0 months between eddies. The eddy shedding in simulation 2 may have a weak contribution from baroclinic instability. *Hurlburt and Thompson* [1982] show that such a contribution can increase the westward propagation speed of the Loop Current

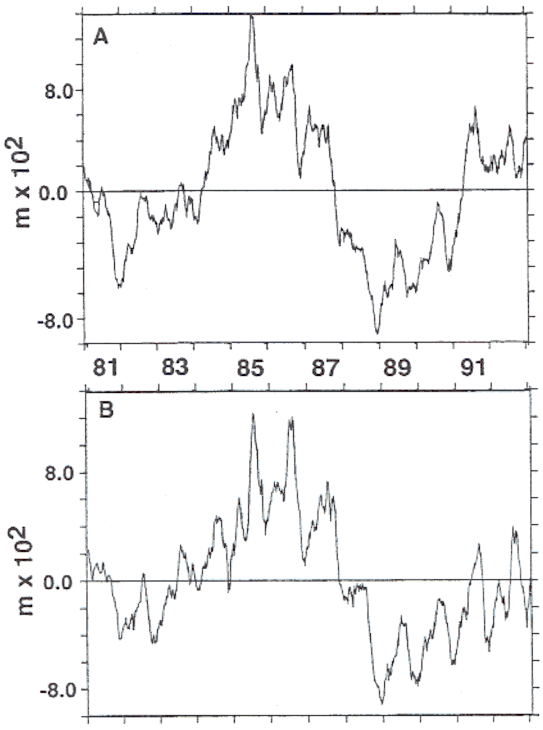

Figure 8. Sum of total upper layer thickness anomaly (meters × 10^2) along the path depicted in Figure 7 for 1981–1992 for (a) simulation 1 and (b) simulation 2. Total track distance is approximately 3800 km.

into an unstable configuration. In their paper the eddy periodicity was about 60 days in simulations where baroclinic instability was dominant. The observed eddy-shedding periods [*Vukovich*, 1995] are much more variable than those exhibited in the model, although 8.3 months matches the primary spectral peaks reported by *Maul et al.* [1985], *Sturges* [1992], and *Vukovich* [1995].

Historically, ring separation was thought to result from seasonal variations in transport through the Yucatan Channel, which affected the penetration distance of the Loop Current into the Gulf of Mexico [*Cochrane*, 1965]. Using a set of numerical simulations, *Hurlburt and Thompson* [1980, 1982] demonstrated that an eddy-shedding period similar to that observed was possible with constant inflow transport. They also demonstrated that a 1.5-layer reduced gravity model was the simplest model that could reproduce the basic eddy-shedding cycle, eliminating baroclinic instability as a determining factor in the periodicity. Instead, they found horizontal shear instability in the first internal mode. It should be noted that while horizontal shear instability was used to explain the final eddy pinch-off in that model, the authors showed that the westward bending of the Loop Current and its tendency to bend back on itself could be understood without invoking an instability mechanism. Thus the eddy-shedding frequency was not determined by a flow instability but, rather, by the time required for the loop to penetrate into the Gulf of Mexico and bend westward into an unstable configuration. This timescale is proportional to the diameter of shed eddies divided by the nondispersive internal Rossby wave speed. The dynamics are discussed in more detail by *Hurlburt and Thompson* [1982, section 5].

3.7. Caribbean Eddies and Loop Current Eddy Shedding

Connections between Loop Current eddy shedding and Caribbean eddies in simulation 1 are evident graphically in Plates 6–8. In addition, a cross correlation between the upper layer thickness time series of increment 27 in the corridor (representing the Loop Current Eddy) and the first increment (representing the initial input of eddies into the Caribbean) shows a significant value of 0.45 at a lag of 11.4 months for simulation 1. Statistical significance was determined using the technique described in the appendix.

A comparison, however, between the five Loop Current eddies shed between March 1984 and November 1987 (the period of high Caribbean eddy activity from Figure 8) and the five eddies shed between December 1987 and March 1991 in simulation 1 (the period of low Caribbean eddy activity from Figure 8) showed no influence of Caribbean eddy activity on the mean eddy-shedding period (8.8 months in both cases). Additionally, there was no significant difference in the average Loop Current eddy propagation speed as determined from Plate 10, nor in eddy diameter measured from the maximum swirl velocity averaged around the eddy. Finally, there was no significant difference in the average maximum swirl velocities. This might not be evident from Plate 10, but note that the background sea surface height was higher during the period of high Caribbean eddy activity. Note that significance was determined by a single classification analysis of variance (ANOVA) [*Sokal and Rohlf*, 1981]. Thus we see Caribbean eddies that (1) cross the entire Caribbean from east to west, (2) squeeze through the Yucatan Channel, (3) influence the strength of the closed anticyclonic circulation inside the Loop Current, and (4) influence the timing of individual eddy-shedding events (including a statistically significant lagged correlation with eddies in the easternmost Caribbean). We do not see, however, a net impact on the mean eddy-shedding period nor on the size or strength of eddies that are shed, a topic which bears further investigation with higher-resolution models.

3.8. Multiyear Anomalies in the Caribbean

A closer examination of Plates 8 and 9 reveals substantial interannual variation in the Caribbean eddy formation and propagation. The sum of the upper layer thickness anomalies along the corridor (Figure 8) shows the extent of this variability. In addition, large interannual variations in the strength of the Caribbean Current are found from the Lesser Antilles to the Yucatan Channel (Figure 9). The mean pattern of a multiyear anomaly where the Caribbean Current strengthened (simulation 1) is depicted in Plate 11a. The variations in the strength of the Caribbean Current and the flow through the Lesser Antilles affect the strength of the mesoscale variability forming in the Caribbean (Plate 8). The anomaly depicted in Plate 11a is mainly confined to the Caribbean and Gulf of Mexico. The part in the central Caribbean, south of Hispaniola and Jamaica, is consistent with a strong anomaly in the regional wind stress curl (Figure 10), with a negative anomaly north of 15°N and a positive anomaly south of 15°N. To further investigate the ocean model's response to this anomaly, the nonlinear results from simulation 1 are compared to corresponding results from a linear simulation (simulation 3), which has an entirely deterministic response to the wind forcing and which tends to adjust toward Sverdrup flow closed by western boundary currents [*Sverdrup*, 1947; *Munk*, 1950]. Compared to the linear solution anomaly (Plate 11b), the nonlinear anomaly

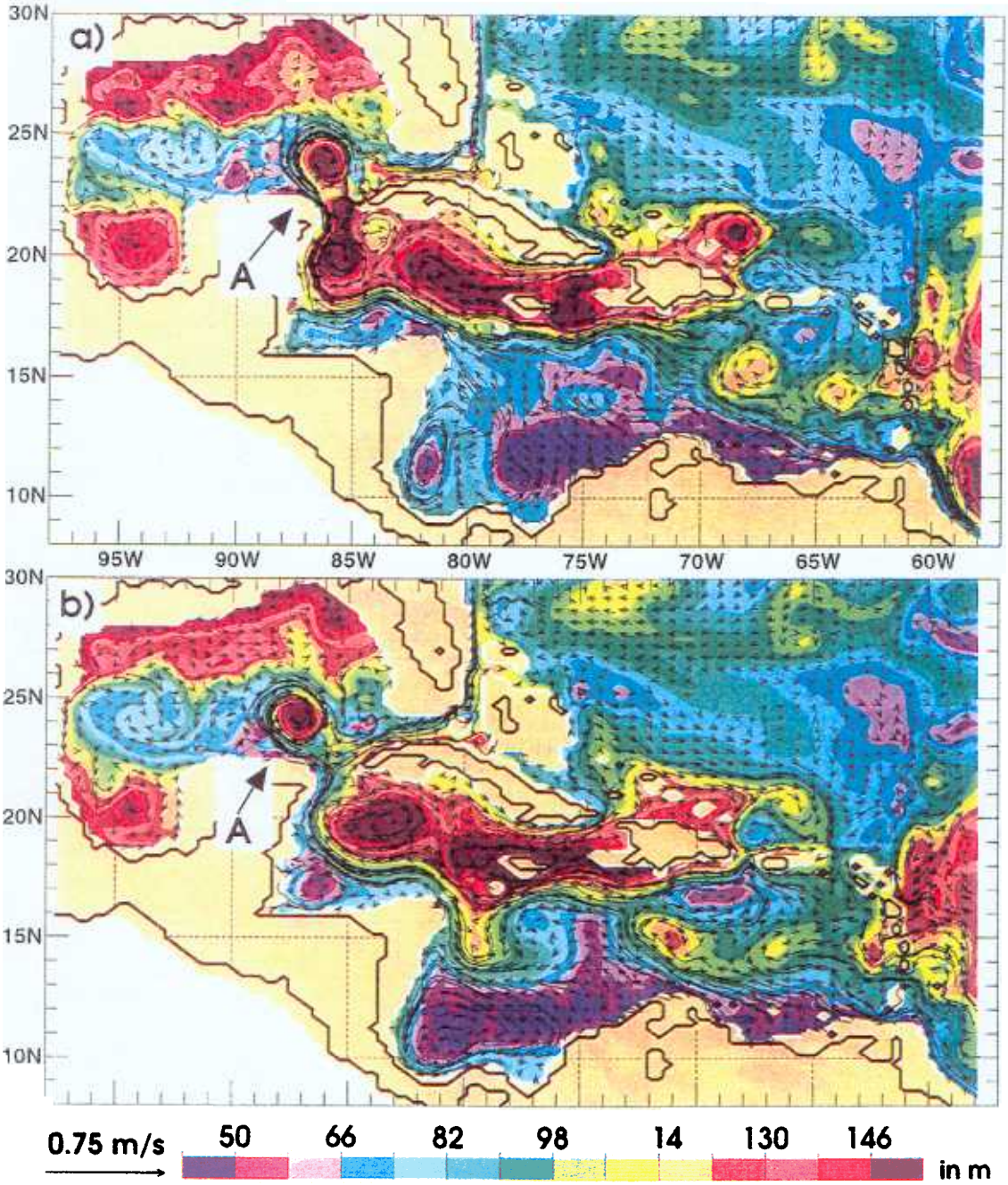

Plate 7. The Loop Current Eddy on (a) July 9, 1992, when it begins to separate, and (b) August 27, 1992, when the Loop Current has shed an eddy.

is stronger in the western Caribbean and extends across the entire Gulf of Mexico (Plate 11a). The westward extension of the anomaly in the nonlinear simulations is a consequence of the strengthened flow instabilities in the Caribbean Current, the associated strong eddy generation, the westward propagation of these eddies, and their ability to squeeze through the Yucatan Channel (Plate 6). Most of these aspects are well illustrated in Plate 8. The comparison of linear and nonlinear anomalies in Plate 11 illustrates the large impact that nonlinearity, flow instabilities, and eddies can have on forced anomalies with much larger space and timescales than mesoscale variability. It also shows the large impact that variability in the Caribbean can have on anomalies in the Gulf of Mexico via nonlinear dynamical mechanisms. As noted in section 3.7, this impact does not affect the mean eddy-shedding period, Loop Current eddy diameter, or maximum swirl velocity. In addition, in the south central Caribbean it shows the ability of these nonlinear dynamics to increase the strength of the cyclonic gyre in the Colombian Basin south of the Caribbean Current.

3.9. Connections to Florida Current Variability

Finally, several cross correlations were calculated between the transport of the Florida Current at 27°N (Subtropical Atlantic Climate Studies (STACS)) and aspects of the circulation in the Caribbean and Gulf of Mexico. These results are reportedly due to the continued interest in understanding the transport variability at 27°N. A cross correlation between transport through the Yucatan Channel and transport at 27°N yielded a

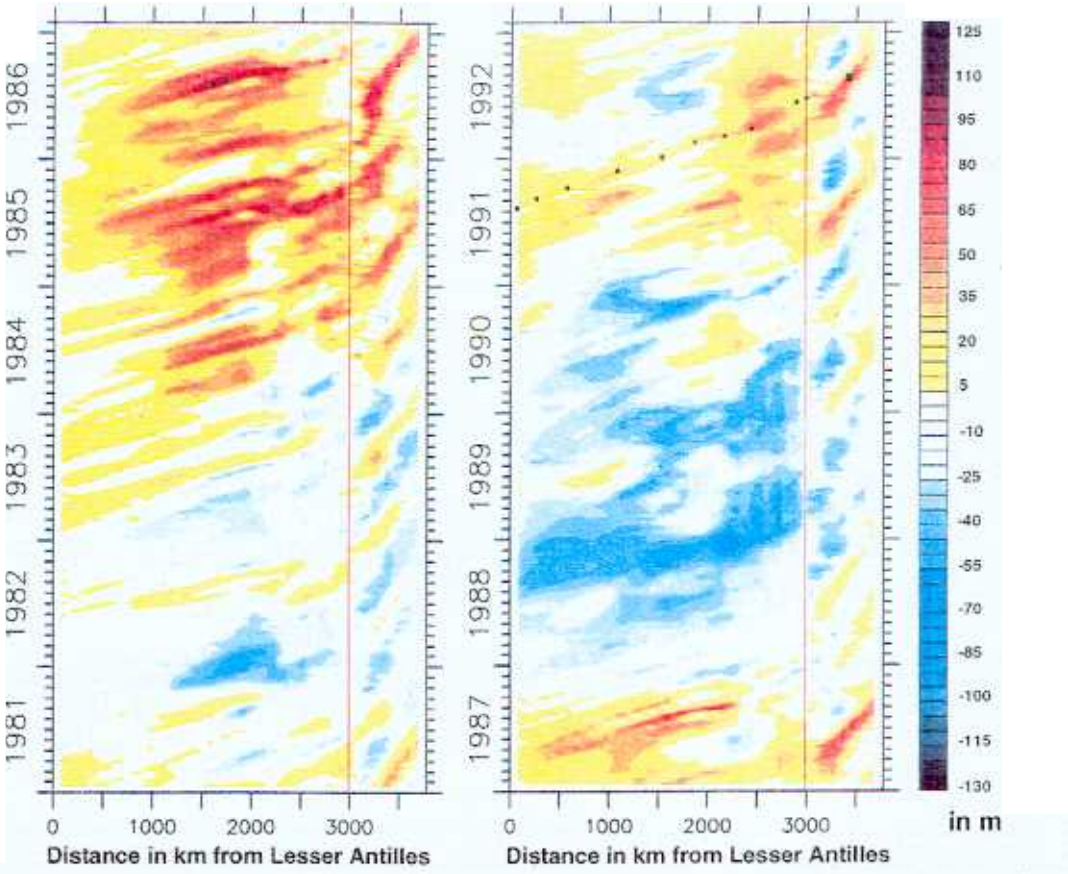

Plate 8. Hopfmuller diagram of upper layer thickness anomaly (meters) versus time from simulation 1 along the path depicted in Figure 7. The x axis is distance in kilometers, with zero being the Lesser Antilles and 3000 km (marked by the red line) denoting the Yucatan Channel

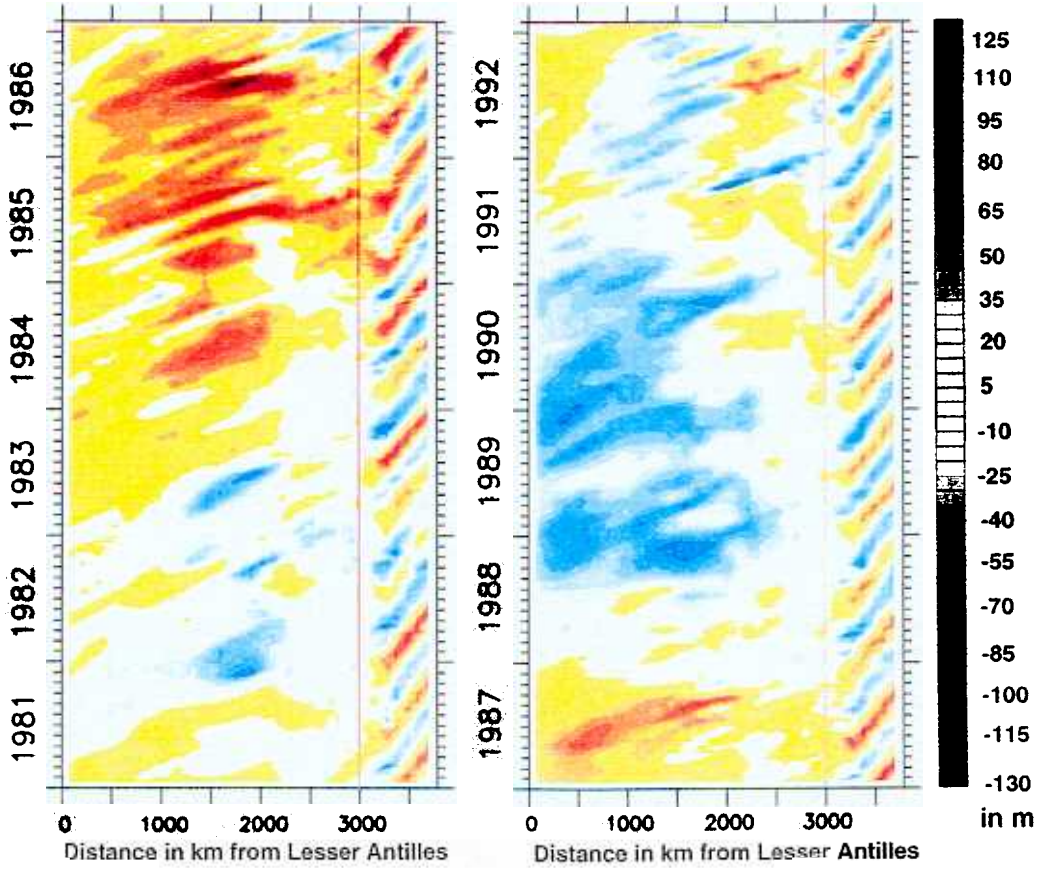

Plate 9. Same as Plate 8, but for simulation 2.

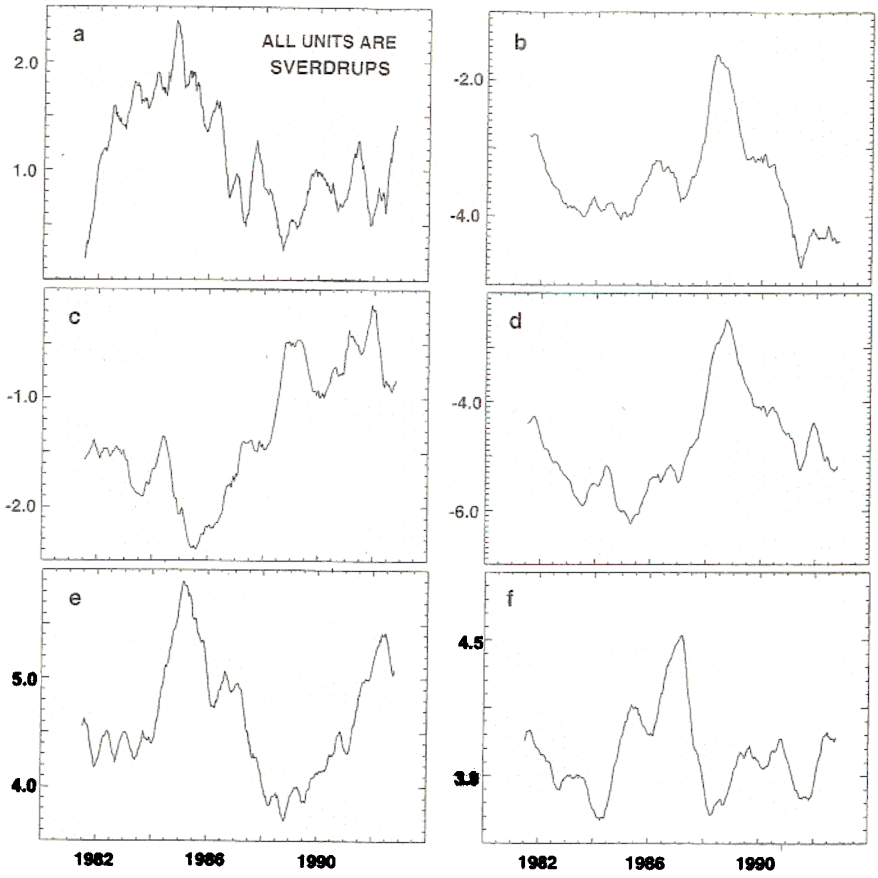

Figure 9. Upper layer transport time series in sverdrups (10^6 m^3 s^{-1}) for various combinations of Caribbean passages from simulation 1. Values were sampled daily and filtered using a 1-year running mean to emphasize interannual variability. (a) Windward plus Mona plus Anegada (northern Caribbean passages), (b) all Lesser Antilles, (c) Guadeloupe plus Dominique plus Martinique (northern passages of the Lesser Antilles), (d) Grenada plus St. Vincent plus St. Lucia (southern passages of the Lesser Antilles), (e) Yucatan Channel, and (f) Florida Current at 27°N.

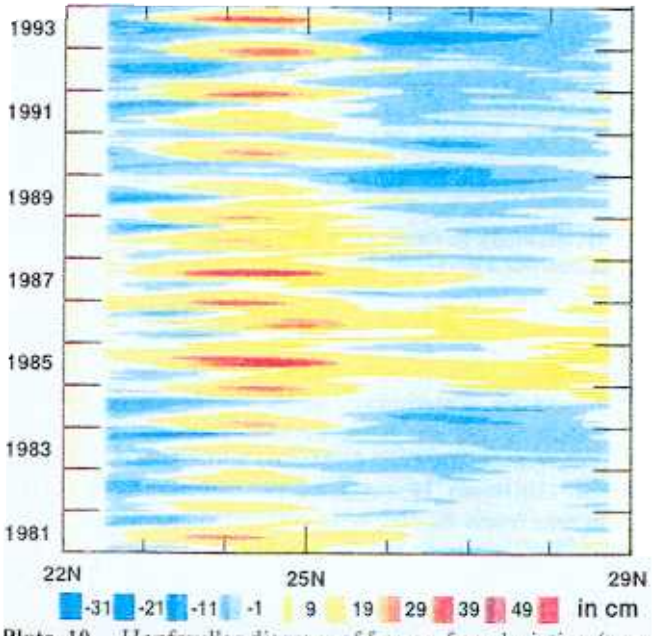

Plate 10. Hopfmuller diagram of free surface deviation (centimeters) versus time at 89.8°W in the Gulf of Mexico showing passage of eddies shed by the Loop Current.

value of 0.64 at a lag of 15 days for simulation 1 and 0.77 at a lag of 15 days for simulation 2. No significant correlation was found between the Loop Current eddy shedding and transport at 27°N.

4. Summary and Conclusions

The connectivity of mesoscale variability in the Atlantic Ocean, Caribbean, and Gulf of Mexico has been studied using three simulations by the Naval Research Laboratory's global ocean model. Two simulations have a horizontal resolution of 1/4° for each variable and include a 5.5-layer reduced gravity and 6-layer finite depth with realistic bottom topography. The third simulation is a linear 1.5-layer reduced gravity, which has horizontal grid resolution of 1/2°. All were forced by daily ECMWF hybrid winds over 1981–1994. Mesoscale features are observed in both of the nonlinear simulations. These features dominate the geostrophically balanced surface layer variability of the Caribbean circulation (Plates 2–7).

The formation of the Caribbean eddies is due in part to potential vorticity that originates in rings from the retroflection of the North Brazil Current (NBC) and that is advected through the Lesser Antilles. This potential vorticity acts as a finite amplitude perturbation for mixed barotropic and internal mode baroclinic instabilities (Plate 2a), and mesoscale fea-

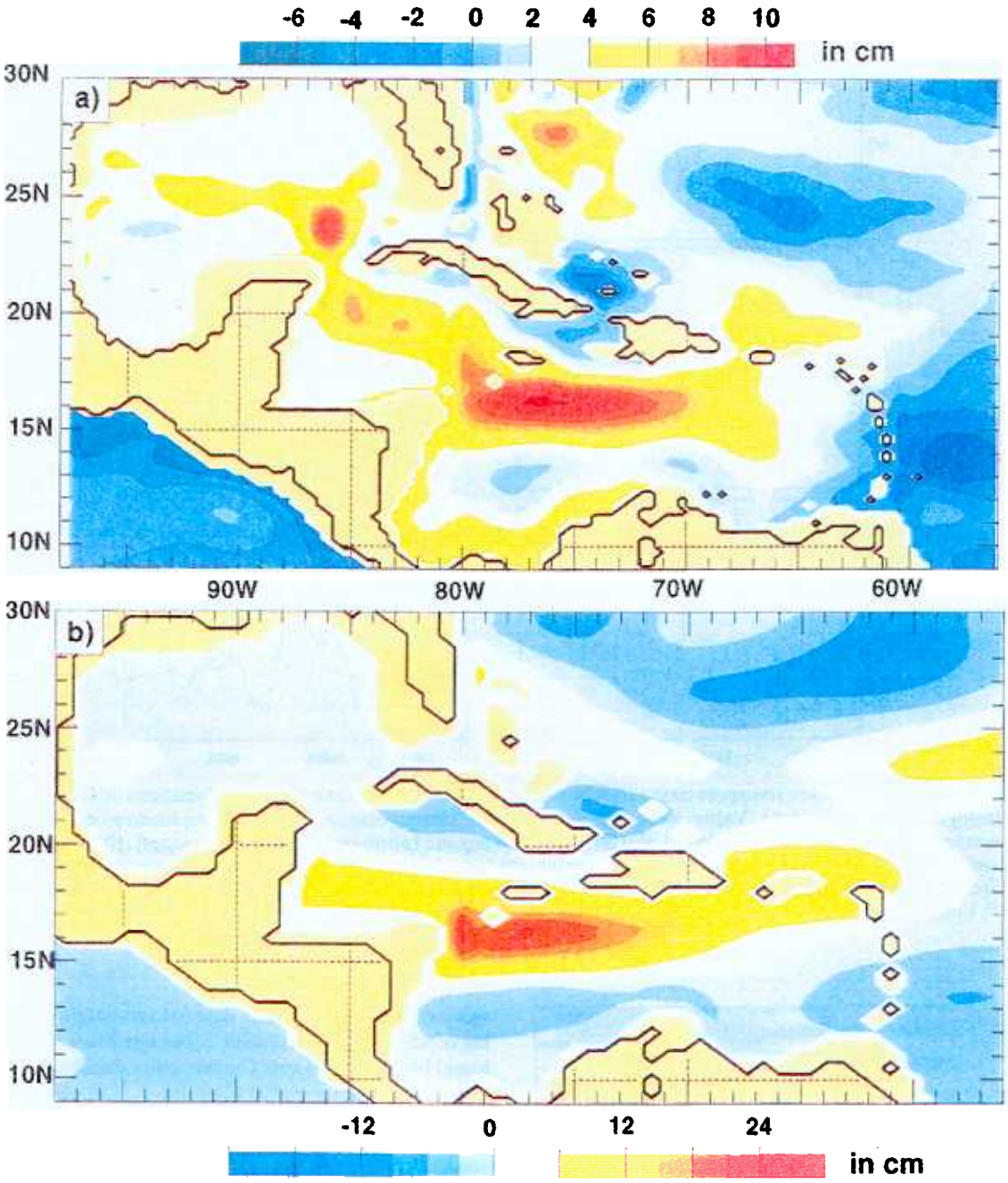

Plate 11. The 1985–1987 mean minus 1981–1991 mean SSH anomaly in centimeters for (a) simulation 1 with a contour interval of 1.0 cm and (b) simulation 3 with a contour interval of 3.0 cm.

tures form as a result. The Caribbean eddies are primarily anticyclonic and transit a fairly narrow corridor westward across the basin (Figure 7) with an average speed of 0.15 m/s. This results in a 10-month travel time from the Lesser Antilles to the Yucatan Channel.

With only limited drifter tracks, satellite altimetry, and sparse hydrographic data, there is a scarcity of observational data in the Caribbean region with which to conduct model-data comparisons. However, eddies similar to those in the model (Figure 5) have been observed by Geosat altimetry [*Nystuen and Andrade*, 1993]. In a model phase plot of upper layer thickness (Plate 8), eddies from the Lesser Antilles can be traced across the Caribbean and through the Yucatan Channel. In addition, a statistically significant (11.4-month lagged) correlation of 0.45 was found between eddy shedding by the Loop Current in the Gulf of Mexico and eddies in the easternmost Caribbean. However, no net influence of Caribbean eddies was found on the mean eddy-shedding period in the Gulf of Mexico nor on the size and strength of shed eddies.

Considerable interannual variation exists in eddy formation and strength. The initial intensity of the Caribbean eddies is weak compared with their NBC counterparts, but as the Caribbean eddies transit the basin, they intensify into larger-scale features (with average diameter of 330 km in simulation 1).

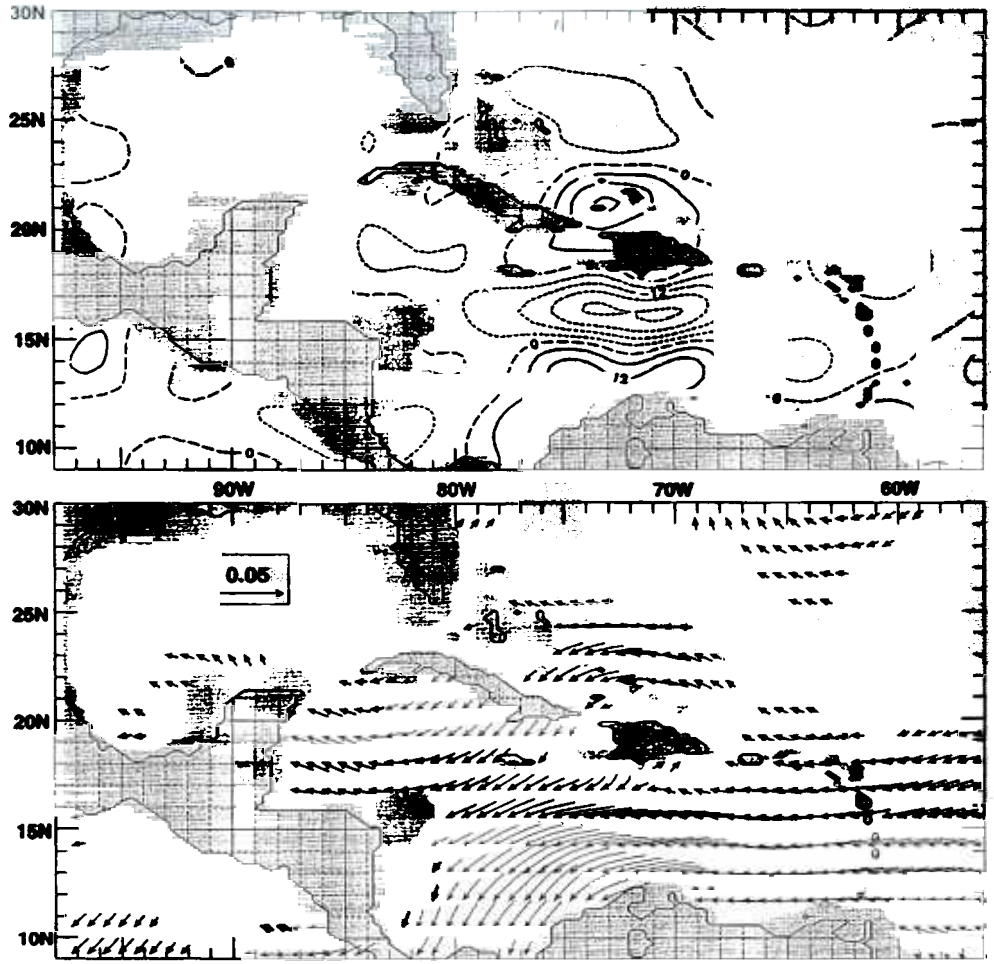

Figure 10. The 1985–1986 mean minus 1981–1991 mean European Centre for Medium-Range Weather Forecasts (a) wind stress curl with contour intervals at 6.0 Pa/m $\times$ 10^{-8} and (b) wind stress in newtons per square meter.

The amount of intensification is strongly affected by interannual variations in the strength of the Caribbean Current, which lies along the axis of eddy propagation (Plate 11a). Similar interannual variability exists in the flow through the Lesser Antilles (Figure 9), which also plays a role in Caribbean eddy strength.

The anomaly depicted in Plate 11a is consistent with a strong anomaly in the regional wind stress curl (Figure 10). The linear simulation, which is forced by the same winds, also depicts an anomaly in the central Caribbean (Plate 11b). A striking difference exists between the areal extent of the anomaly in the linear and nonlinear simulations. The nonlinear anomaly (simulation 1) is stronger in the western Caribbean and extends across the entire Gulf of Mexico. The anomaly in the linear simulation (simulation 3) is confined to the Caribbean. This difference is a consequence of the flow instabilities in the Caribbean Current, the associated eddy generation, the westward propagation of the eddies, and their ability to squeeze through the Yucatan Channel (Plate 6).

Both nonlinear simulations show similar complex eddy fields. These simulations were forced by daily winds for 14 years. The variability of these winds greatly enhanced the Caribbean mesoscale variability over a similar global simulation forced by Hellerman and Rosenstein climatological winds. The latter exhibited significantly less eddy kinetic energy in the Caribbean (E. J. Metzger, personal communication, 1995).

A Caribbean model that is forced by a constant inflow through the Lesser Antilles [*Heburn et al.*, 1982] can produce some eddies but does not capture the periodicity, connectivity, or cycles of Caribbean eddies. Even prescribing a variable inflow similar to the transports observed in the model (Figure 9) would mask the dynamical contributions of the Atlantic, unless they came from an Atlantic model. Any successful modeling of Caribbean variability must therefore consider the influence of the Atlantic.

The results of this study depend on the ability of the model to represent the necessary mesoscale variability and the geometry of the islands surrounding the Caribbean, especially the Lesser Antilles island arc. With higher model resolution one would expect greater mesoscale variability and more accurate representation of the island arc. However, great care was exercised in representing the island arc present in the model and detailed maps were used to make many improvements over the standard ETOP05 topography used by most ocean modelers. These results show that the model represents the geometry well enough and has sufficient variability to demonstrate the main features of interest, including (1) production of strong rings from the retroflection of the North Brazil Current, (2)

connectivity between NBC rings and eddy generation in the eastern Caribbean that is strongly affected by the Lesser Antilles, (3) strong mesoscale variability with the Caribbean, (4) eddies that transit the entire Caribbean and amplify in the process owing to flow instabilities, and (5) eddy shedding in the Gulf of Mexico. Accurate representation of the island arc is critical. In the present study the NBC rings decay on the eastern side of the Lesser Antilles because the island arc serves as a barrier to propagation into the Caribbean. If the Lesser Antilles were eliminated or represented with unrealistically large gaps, the NBC rings could continue a northwestward pathway into the Caribbean unimpeded.

As described earlier, we find a less direct influence of NBC rings in the Caribbean and Gulf of Mexico because some potential vorticity from the rings is advected into the Caribbean through passages of the Lesser Antilles, providing finite amplitude perturbations for flow instabilities within the Caribbean. In the model this impact is sufficient to yield a significant correlation (0.45) between eddy shedding in the Gulf of Mexico and eddies near the Lesser Antilles. However, no significant correlation is found between eddy shedding in the Gulf of Mexico and transport variations in the Straits of Florida, although the correlation between transport fluctuations in the Yucatan Channel and the Straits of Florida at 27°N is about 0.7 with a lag of 15 days.

Appendix: Significance Test

Given two time series $T(j)$ and $S(j)$ (where $j = 1, N$ and N is the total number of observations) and their time-lagged cross-correlation function CCF$(-L, +L)$ (L is maximum lag), a significance test on CCF can be conducted using the following procedure: first, compute the autocorrelation function a of T; second, calculate surrogate T time series STS by

$$\mathrm{STS}(j) = a\mathrm{STS}(j) + k(j) \qquad \text{(A1)}$$

where k is a random number between 0 and 1 and $j = 1,1000$. The surrogate time series preserves the autocorrelation function of the original function, and the addition of k is equivalent to the addition of random noise.

Third, calculate the cross-correlation function between each of the surrogate time series and the other original series S and rank the values in ascending order by lag. The 975th and 25th rankings represent two-tailed 95% confidence limits about the original CCF.

The addition of random numbers is frequently used in Monte Carlo techniques [*Hammersley and Handscomb*, 1964] to create surrogate time series. The ranked correlations between the surrogate and S represent the highest values one would statistically expect for a correlation with noise. Therefore, if the original CCF is higher than a correlation for noise, it is considered significant.

Acknowledgments. This work was performed as part of the 6.1 project Dynamics of Low Latitude Western Boundary Currents. It is also a contribution to the 6.2 Global Ocean Prediction System project, modeling task, as part of the Naval Ocean Modeling and Prediction (NOMP) program. The Office of Naval Research (ONR) sponsored these two projects under program elements 60115N and 62435N, respectively. The ocean model simulations were run by E. Joseph Metzger and performed on the CRAY Y-MP 8/8128 at the Naval Oceanographic Office, Stennis Space Center, Mississippi, and the CRAY C90/161024 at the Army Corps of Engineers Waterways Experiment Station, Vicksburg, Mississippi. The C90 was used under a computer time grant from the Defense Department High Performance Computing Initiative. James J. O'Brien received support from the Physical Oceanography Program of ONR under the Secretary of the Navy Chair Grant. Sylvia Murphy split her effort between Florida State University and NRL during the conduct of this research and was supported by an NRL fellowship while at Florida State. We thank Tamara L. Townsend for her helpful comments and suggestions, Alan J. Wallcraft for his work on developing of the NRL global ocean model, and Ashley McManus for her assistance with the figures. This work is NRL contribution JA/7322-96-0030.

References

Cochrane, J. D., The Yucatan Current and equatorial currents of the western Atlantic, *Ref. (65-17T)*, pp. 20–27, Dep. of Oceanogr., Tex. A&M Univ., College Station, 1965.

Didden, N., and F. Schott, Eddies of the North Brazil Current retroflection region observed by Geosat altimetry, *J. Geophys. Res.*, *98*, 20,121–20,131, 1993.

Duncan, C. P., S. G. Schladow, and W. G. Williams, Surface currents near the Greater and Lesser Antilles, *Int. Hydrogr. Rev.*, *LIX*(2), 67–78, 1982.

European Centre for Medium-Range Weather Forecasts (ECMWF), The description of the ECMWF/WCRP level III—A global atmospheric data archive, report, 72 pp., Reading, England, 1994.

Fratantoni, D. M., W. E. Johns, and T. L. Townsend, Rings of the North Brazil Current: Their structure and behavior inferred from observations and a numerical simulation, *J. Geophys. Res.*, *100*, 10,633–10,654, 1995.

Fu, L. L., and B. Holt, Some examples of detection of oceanic mesoscale eddies by the SEASAT synthetic-aperture radar, *J. Geophys. Res.*, *88*, 1844–1852, 1983.

Hammersley, J. M., and D. C. Handscomb, *Monte Carlo Methods*, 178 pp., Chapman and Hall, New York, 1964.

Heburn, G. W., T. H. Kinder, J. H. Allender, and H. E. Hurlburt, A numerical model of eddy generation in the southeastern Caribbean Sea, in *Hydrodynamics of Semi-Enclosed Seas*, edited by J. C. J. Nihoul, pp. 299–328, Elsevier Sci., New York, 1982.

Hellerman, S., and M. Rosenstein, Normal monthly wind stress over the world ocean with error estimates, *J. Phys. Oceanogr.*, *13*, 1093–1104, 1983.

Hurlburt, H. E., and J. D. Thompson, A numerical study of Loop Current intrusions and eddy shedding, *J. Phys. Oceanogr.*, *10*, 1611–1651, 1980.

Hurlburt, H. E., and J. D. Thompson, The dynamics of the Loop Current and shed eddies in a numerical model of the Gulf of Mexico, in *Hydrodynamics of Semi-Enclosed Seas*, edited by J. C. J. Nihoul, pp. 243–297, Elsevier Sci., New York, 1982.

Hurlburt, H. E., and J. D. Thompson, Preliminary results from a numerical study of the New England Seamount Chain influence on the Gulf Stream, in *Predictability of Fluid Motions*, edited by G. Holloway and B. J. West, pp. 489–504, Am. Inst. of Phys., College Park, Md., 1984.

Hurlburt, H. E., and T. L. Townsend, NRL efforts in the North Atlantic, in *Data Assimilation and Model Evaluation Experiments—North Atlantic Basin: Preliminary Experiment Plan*, edited by R. C. Willems, pp. 30–39, Cent. for Ocean Atmos. Modeling, Univ. of South. Miss., Stennis Space Center, 1994.

Hurlburt, H. E., A. J. Wallcraft, W. J. Schmitz Jr., P. J. Hogan, and E. J. Metzger, Dynamics of the Kuroshio/Oyashio current system using eddy-resolving models of the North Pacific Ocean, *J. Geophys. Res.*, *101*, 941–976, 1996.

Ingham, M. C., and C. V. W. Mahnken, Turbulence and productivity near St. Vincent Island, BWI, A preliminary report, *Caribbean J. Sci.*, *6*(3–4), 83–87, 1966.

Jacobs, G. A., H. E. Hurlburt, J. C. Kindle, E. J. Metzger, J. L. Mitchell, W. J. Teague, and A. J. Wallcraft, Decade-scale trans-Pacific propagation and warming effects of an El Nino anomaly, *Nature*, *370*, 360–363, 1994.

Johns, W. E., T. N. Lee, F. A. Schott, R. J. Zantopp, and R. H. Evans, The North Brazil Current retroflection: Seasonal structure and eddy variability, *J. Geophys. Res.*, *95*, 22,103–22,120, 1990.

Kinder, T. H., Shallow currents in the Caribbean Sea and the Gulf of Mexico as observed with satellite-tracked drifters, *Bull. Mar. Sci.*, *33*, 239–246, 1983.

Kinder, T. H., G. W. Heburn, and A. W. Green, Some aspects of the Caribbean Circulation, *Mar. Geol.*, *68*, 25–52, 1985.

Larsen, J. C., Transport and heat flux of the Florida Current at 27°N derived from cross-stream voltages and profiling data: Theory and observations, *Philos. Trans. R. Soc. London, Ser. A*, *338A*, 169–236, 1992.

Leipper, D. F., A sequence of current patterns in the Gulf of Mexico, *J. Geophys. Res.*, *75*, 937–948, 1970.

Lemming, T. D., Eddies west of the Southern Lesser Antilles, in *Symposium on Investigations and Resources of the Caribbean Sea and Adjacent Regions*, pp. 113–120, UNESCO, Paris, 1971.

Levitus, S., Climatological atlas of the world ocean, *NOAA Prof. Pap. 13*, 173 pp., U.S. Govt. Print. Off., Washington, D. C., 1982.

Maul, G. A. (Ed.), *Climate Change in the Intra-Americas Sea*, 389 pp., Chapman and Hall, New York, 1993.

Maul, G. A., and F. M. Vukovich, The relationship between variations in the Gulf of Mexico Loop Current and the Straits of Florida volume transport, *J. Phys. Oceanogr.*, *23*, 785–796, 1993.

Maul, G. A., D. A. Mayer, and S. R. Baig, Comparisons between a continuous 3-year current-meter observation at the sill of the Yucatan Strait, satellite measurements of Gulf Loop Current area, and regional sea level, *J. Geophys. Res.*, *90*, 9089–9096, 1985.

Mazeika, P. A., T. H. Kinder, and D. A. Burns, Measurements of subtidal flow in the Lesser Antilles passages, *J. Geophys. Res.*, *88*, 4483–4488, 1983.

McWilliams, J. C., and G. R. Flierl, On the evolution of isolated nonlinear vortices, *J. Phys. Oceanogr.*, *9*, 1155–1182, 1979.

Mesinger, F., and A. Arakawa, Numerical methods used in atmospheric models, *GARP Publ. Ser. 17*, 64 pp., World Meteorol. Organ., Geneva, 1976.

Metcalf, W. G., M. C. Stalcup, and M. E. Zemanovic, Hydrographic station data from Atlantis II cruise 56 to the southeastern approaches to the Caribbean Sea, February–April 1970, *Tech. Rep. WHOI-71-13*, Woods Hole Oceanogr. Inst., Woods Hole, Mass., 1971.

Metzger, E. J., H. E. Hurlburt, J. C. Kindle, Z. Sirkes, and J. M. Pringle, Hindcasting of wind-driven anomalies using a reduced-gravity global ocean model, *Mar. Technol. Soc. J.*, *26*(2), 23–32, 1992.

Molinari, R. L., M. Spillane, I. Brooks, D. Atwood, and C. Duckett, Surface currents in the Caribbean Sea as deduced from Lagrangian observations, *J. Geophys. Res.*, *86*, 6537–6542, 1981.

Munk, W. H., On the wind-driven ocean circulation, *J. Meteorol.*, *7*, 79–93, 1950.

National Oceanic and Atmospheric Administration, ETOP05 digital relief of the surface of the earth, *Data Announce. 86-MGG-07*, Natl. Geophys. Data Cent., Washington, D. C., 1986.

Nystuen, J. A., and C. A. Andrade, Tracking mesoscale ocean features in the Caribbean Sea using Geosat altimetry, *J. Geophys. Res.*, *98*, 8389–8394, 1993.

Richardson, P. L., G. E. Hufford, R. Limeburner, and W. S. Brown, North Brazil Current retroflection eddies, *J. Geophys. Res.*, *99*, 5081–5093, 1994.

Roemmich, D., Circulation of the Caribbean Sea: A well resolved inverse problem, *J. Geophys. Res.*, *86*, 7993–8005, 1981.

Schmitz, W. J., Jr., On the interbasin-scale thermohaline circulation, *Rev. Geophys.*, *33*(2), 151–173, 1995.

Schmitz, W. J., Jr., On the world ocean circulation, vol. 1, Some global features/North Atlantic Circulation, *Tech. Rep. WHOI-96-03*, Woods Hole Oceanogr. Inst., Woods Hole, Mass., 1996.

Schmitz, W. J., Jr., and P. L. Richardson, On the sources of the Florida Current, *Deep Sea Res., Part A*, *38*, supp. 1, S379–S409, 1991.

Shriver, J. F., and H. E. Hurlburt, The contribution of the global thermohaline circulation to the Pacific to Indian Ocean throughflow via Indonesia, *J. Geophys. Res.*, *102*, 5491–5511, 1997.

Sokal, R. R., and F. J. Rohlf, *Biometery*, 859 pp., W. H. Freeman, New York, 1981.

Stalcup, M. C., and W. G. Metcalf, Current measurements in the passages of the Lesser Antilles, *J. Geophys. Res.*, *77*, 1032–1049, 1972.

Stalcup, M. C., W. G. Metcalf, and M. E. Zemanovic, Current measurements in the Lesser Antilles, *Tech. Rep. WHOI-71-51*, Woods Hole Oceanogr. Inst., Woods Hole, Mass., 1971.

Sturges, W., The spectrum of Loop Current variability from gappy data, *J. Phys. Oceanogr.*, *22*, 1245–1256, 1992.

Sverdrup, H. U., Wind-driven currents in a baroclinic ocean; With application to the equatorial currents of the eastern Pacific, *Proc. Natl. Acad. Sci. U. S. A.*, *33*, 318–326, 1947.

Toggweiler, J. R., and B. Samuels, New radiocarbon constraints on the upwelling of abyssal water to the oceans surface, in *The Global Carbon Cycle, NATO ASI Ser., Ser. I*, vol. 15, edited by M. Heimann, pp. 303–331, Springer-Verlag, New York, 1993.

Vukovich, F. M., Loop Current boundary variations, *J. Geophys. Res.*, *93*, 15,585–15,591, 1988.

Vukovich, F. M., An updated evaluation of the Loop Current's eddy-shedding frequency, *J. Geophys. Res.*, *100*, 8655–8659, 1995.

Wallcraft, A. J., The Navy Layered Ocean Model Users Guide, *NOARL Rep. 35*, 21 pp., Nav. Res. Lab., Stennis Space Cent., Miss., 1991.

Wilson, W. D., and W. E. Johns, Velocity structure and transport in the Windward Island Passages, *Deep Sea Res., Part I*, *44*, 487–520, 1997.

Youtsey, W. J., Report detailing modifications to the 1/8 degree global bathymetry, Sverdrup Technol. Inc., Stennis Space Cent., Miss., 1993.

H. E. Hurlburt and S. J. Murphy, Naval Research Laboratory, Code 7320, Stennis Space Center, MS 39529. (murphy@nrlssc.navy.mil)

J. J. O'Brien, Center for Atmospheric Prediction Studies, 2035 East Paul Dirac Drive, R. M. Johnson Building, Suite 200, Tallahassee, FL 32310.

(Received March 6, 1998; revised August 13, 1998; accepted August 31, 1998.)